Available online at www.sciencedirect.com
ScienceDirect
Journal of Computational Physics 220 (2006) 471–497
JOURNAL OF COMPUTATIONAL PHYSICS
www.elsevier.com/locate/jcp

Piecewise linear discretization of Symbolic Implicit Monte Carlo radiation transport in the difference formulation ☆

Eugene D. Brooks III *, Abraham Szőke, Jayson D.L. Peterson

University of California, Lawrence Livermore National Laboratory, P.O. Box 808, Livermore, CA 94550, USA

Received 7 December 2005; received in revised form 13 July 2006; accepted 14 July 2006
Available online 7 September 2006

Abstract

We describe a Monte Carlo solution for time dependent photon transport, in the difference formulation with the material in local thermodynamic equilibrium, that is piecewise linear in its treatment of the material state variable. Our method employs a Galerkin solution for the material energy equation while using Symbolic Implicit Monte Carlo to solve the transport equation. In constructing the scheme, one has the freedom to choose between expanding the material temperature, or the equivalent black body radiation energy density at the material temperature, in terms of finite element basis functions. The former provides a linear treatment of the material energy while the latter provides a linear treatment of the radiative coupling between zones. Subject to the conditional use of a lumped material energy in the vicinity of strong gradients, possible with a linear treatment of the material energy, our approach provides a robust solution for time dependent transport of thermally emitted radiation that can address a wide range of problems. It produces accurate results in thick media.

Keywords: Difference formulation; Radiation transport; Implicit Monte Carlo

1. Introduction

In earlier work [1,2], some of the authors introduced the difference formulation for photon transport, under conditions of local thermodynamic equilibrium (LTE) for the material, and demonstrated a significant gain in computational efficiency for a Symbolic Implicit Monte Carlo (SIMC) [3,4] implementation for optically thick media. In order to obtain accurate results, the zone size for this piecewise constant implementation is limited to about one mean free path. The cause of this limitation is energy teleportation

☆ This work was performed under the auspices of the US Department of Energy by the University of California, Lawrence Livermore National Laboratory under Contract No. W-7405-Eng-48.
* Corresponding author. Tel.: +1 925 423 7341; fax: +1 925 423 8086.
E-mail address: brooks3@llnl.gov (E.D. Brooks III).

0021-9991/$ - see front matter
doi:10.1016/j.jcp.2006.07.014

[5], wherein energy that is absorbed on one side of a zone is immediately re-emitted on the opposite side. This defect causes a faster-than-physical propagation velocity for a Marshak (thermal) wave, and excessive energy transport even under steady state conditions.

Densmore and Larsen [6] have shown that the local coupling of the radiation and the material energy is correct in the Symbolic Implicit Monte Carlo method, and in the context of their analysis the SIMC method has the diffusion limit, but they did not consider the impact of the spatial discretization of the material state variable. Clouet and Samba [7] have shown that a piecewise linear discretization of the material state variable produces the correct diffusion limit, while a piecewise constant treatment of the material state variable does not. They did this in the context of a linearized form of the grey transport problem [8], for a time independent solution. As they used the standard formulation of transport, Monte Carlo noise was an issue that led them to the conclusion that practical application of their extension of the SIMC method might be limited by the noise problem. For an extended discussion of what is meant when a discretization of the transport equation has the diffusion limit, refer to [9].

The method of Clouet and Samba is based on a Galerkin [10] solution of the material energy equation and uses a piecewise linear finite element basis that permits discontinuities at interior zone edges in order to represent the material state variable within a zone. In this paper, we extend the method of Clouet and Samba to the time dependent solution of the non-linear equations of LTE transport in the difference formulation, using piecewise linear basis functions, in slab geometry.

A significant difficulty that occurs in the standard formulation of transport when attempting to extend SIMC with a finite element treatment of the material state variable is that of correctly sampling the source term. Correct sampling of the emission spectrum, when it depends upon the details of the material opacity at the temperature of the position sampled, requires an integral of the opacity against the Planck distribution function for each particle sampled. In the difference formulation, the thermal emission in a zone does not depend on the material opacity and this difficulty does not occur.

In addressing the non-linear equations of time dependent radiation transport, one has a choice between representing the temperature, T, or the equivalent black body radiation energy density at the material temperature, $\Phi = aT^4$, using finite element basis functions. In the former, the material energy is linear when a constant specific heat is used during a time step while the radiative coupling between zones is not. In the latter, the radiative coupling between zones is linear while the material energy, expressed in terms of Φ, is not. Linear treatment of Φ produces the best accuracy near steady state, while linear treatment of the material temperature produces the best accuracy when the problem contains violent time dependent behavior. This will become clear in the numerical results presented in this paper.

A time dependent, self-consistent, piecewise linear solution of radiation transfer becomes non-monotonic in the vicinity of a strong gradient. When a thermal wave impinges on one side of an optically thick zone, the self-consistent solution of the energy equation drives the far side down in temperature, even though the energy absorbed there is positive (but small). This problem becomes particularly serious when the initial temperature of the material is small, as it can lead to negative temperature excursions that stop the calculation. The technique of lumping the material energy (or mass) matrix [10] is a method used to address this problem in conventional applications of the finite element method. We find lumping to be a useful means of avoiding the monotonicity problem in the context of transport for thermally emitted photons. However, lumping reduces the accuracy of the solution in the affected zones. It gets the average temperature correct, but introduces an error in the slope of a time dependent solution that would otherwise be accurate.

In Section 2 we briefly describe the difference formulation for the transport of photons, under conditions of local thermodynamic equilibrium, in the slab geometry environment that we will use for our exposition in this paper. In Section 3, we sketch the solution method, and refer to other sections of the paper that provide extensive details of the implementation. We provide numerical results in Sections 8 and 9, documenting the characteristics of the method for problems involving an optical thickness of one mean free path per zone. In Section 11 we demonstrate the performance of the method for a thermal wave penetration problem that is optically thick, comparing its behavior to that of the piecewise constant treatment of the material state variable. We provide a discussion in Section 12. The intervening sections and appendices of this paper delve into the significant details of our method.

2. The difference formulation

We want to solve the coupled equations for photon transport, Eq. (1) shown below, and the material energy, Eq. (2), in the difference formulation. In this model for photon transport the interaction of the radiation with the material (absorption and thermal emission) is accomplished using the simplifying assumption of local thermodynamic equilibrium (LTE) for the material degrees of freedom. For the purpose of this paper we restrict the problem to slab geometry, exclude physical scattering, and assume that the material is stationary. Lifting these restrictions poses no significant difficulties for the Monte Carlo solution method we describe. We have exposed the independent variables in the equations below for clarity:

$$\frac{1}{c}\frac{\partial D(x,t;v;\mu)}{\partial t}+\mu\frac{\partial D(x,t;v;\mu)}{\partial x}=-\sigma'_a(v,T(x,t))D(x,t;v;\mu)-\frac{1}{c}\frac{\partial B(v,T(x,t))}{\partial t}-\mu\frac{\partial B(v,T(x,t))}{\partial x}, \tag{1}$$

$$\frac{\partial E_{\mathrm{mat}}(T(x,t))}{\partial t}=2\pi\int_0^\infty \mathrm{d}v\int_{-1}^{1}\mathrm{d}\mu\sigma'_a(v,T(x,t))D(x,t;v;\mu)+G(x,t), \tag{2}$$

where $G(x,t)$ is a prescribed energy source.

The field that is transported, D, is the difference between the specific intensity for photons, I, and the black body distribution at the material temperature, $B(v,T(x,t))$; that is $I=D+B$ provides the relationship between the difference formulation and the standard formulation for photon transport with the material in LTE. It also provides a means for mapping boundary conditions between the two formulations. It is useful to note that the opacity corrected for stimulated emission, σ'_a, the material energy, E_{mat}, and the local blackbody field, B, are indirect functions of space and time through their dependence on the temperature, $T(x,t)$. This becomes important when the temperature, $T(x,t)$, is a function of space during a time step.

We define the black body radiation energy density, $\Phi=aT^4$, where a is the radiation constant. The factorization of B into a strength times a frequency distribution function gives

$$B(v,T)=\frac{caT^4}{4\pi}b(v,T), \tag{3}$$

with

$$\int_0^\infty b(v,T)\,\mathrm{d}v=1,\quad b(v,T)>0. \tag{4}$$

Equivalently, one can express B in terms of Φ,

$$B(v,\Phi)=\frac{c\Phi}{4\pi}b(v,\Phi). \tag{5}$$

The source terms in the radiation transport equation for the difference field, D, can be factored using the chain rule, giving

$$-\frac{1}{c}\frac{\partial B}{\partial t}-\mu\frac{\partial B}{\partial x}=\frac{4\pi}{c}\frac{\partial B}{\partial \Phi}\left[-\frac{1}{4\pi}\frac{\partial \Phi(x,t)}{\partial t}-\frac{\mu c}{4\pi}\frac{\partial \Phi(x,t)}{\partial x}\right]=\frac{4\pi}{ca}\frac{\partial B}{\partial T^4}\left[-\frac{aT^3}{\pi}\frac{\partial T}{\partial t}-\frac{\mu caT^3}{\pi}\frac{\partial T}{\partial x}\right]. \tag{6}$$

The use of the chain rule to factor the source terms in the difference formulation is the equivalent of the factorization of the Planck distribution, Eq. (3), used in the standard formulation of SIMC transport. The term $(4\pi/c)(\partial B/\partial\Phi)$ is a frequency distribution function, it is positive and its frequency integral is unity. The sampling of this frequency distribution was dealt with in detail in the appendix of [2] and is further refined for the finite difference case in Appendix B of this paper. The linearity of the strength of the source terms when written as a function of Φ, and the non-linearity of the strength of the source terms when written as a function of T, is clear in Eq. (6).

3. Solution method

The sections that follow contain a detailed account of the implementation of our solution of Eqs. (1) and (2), using a SIMC method that employs a piecewise linear finite element treatment of the material

state variable. Our method is similar to that of Clouet and Samba [7]. In a nutshell, our algorithm is organized as follows:

- The material state variable is represented by a finite element expansion in space. The time dependence is given by the time dependence of the expansion coefficients.
- The source terms of the transport equation, which depend only upon the material state variable and no other physical properties, are factored in terms of space, angle, and frequency distributions that are known at the beginning of the time step (explicit treatment) and in terms of a strength that depends upon coefficients of the finite element expansion that will not be known until the end of the time step (implicit treatment).
- The source terms are sampled and the transport equation is solved by a Monte Carlo simulation that propagates these sources, which carry the unknown strength terms symbolically, along with any census particles, which carry weights determined in a prior time step, to the end of the current time step.
- The equation for the change to the material energy is projected onto the basis functions (a Galerkin projection [10]). This produces a set of non-linear algebraic equations that relate the unknown coefficients of the finite element expansion for the material state variable.
- The set of equations for the material state variable is solved, and the solution is then used to resolve the unknown factors in the census particle list in order to prepare the initial conditions for the next time step.

In addition to the finite element basis employed by Clouet and Samba that admits discontinuities at the interfaces of interior zones, we also demonstrate a modification of this basis that enforces continuity of the solution on interior zone interfaces. The finite element basis we use is described in Section 4 and our method of collapsing to a basis that enforces continuity is described in Section 10.

The underlying SIMC method is based on the idea of factoring the source terms into space, time, frequency and angular distributions that are known at the beginning of the time step (treated explicitly), and strength that depends upon the radiation energy density, $\Phi = aT^4$, that will not be known until the end of the time step (treated implicitly). This allows the source terms to be sampled in space, time, and frequency while leaving the weights of the Monte Carlo particles unknown. The transport equation is then solved in terms of the unknown values of the material state variable by Monte Carlo simulation. The source particle sampling in this paper is substantially complicated by the piecewise linear treatment of the material state variable. This is described at length in Section 6 as well as in the appendix.

As the Monte Carlo particles propagate they lose their energy to the matter. This energy deposition, along with material equation of state and heating terms, must be accounted for in the solution of the material energy equation. We use the Galerkin method in order to solve for the material state variable at the end of the time step. In the Galerkin method, a set of algebraic equations for the material state variable is generated by projecting the material energy equation onto the basis functions. By using this solution strategy, we restrict the solution for the material state variable to be a member of the space of functions spanned by the piecewise linear basis. This is discussed in Section 7.

The set of algebraic equations produced by the Galerkin projection of the energy equation is non-linear in the unknown coefficients of the finite element expansion for the material state variable at the end of the time step. We resort to Newton–Raphson iteration to solve this set of equations, employing the known material state values at the start of the time step as the starting point. For each iteration of the solver, the Newton–Raphson solution of the energy equation requires the Galerkin projection of the energy equation and its partial derivatives with respect to the unknown material state variable. The partial derivatives are evaluated analytically, instead of numerically, and the consistency of the Galerkin projection and its partial derivatives is of paramount importance to the robustness of the solver. Although we do not document these issues completely, enough key details are described in Section 7 that our results can be reproduced.

Once the solution for the material state variable is known, the unknown factors for the weights of Monte Carlo particles born during the time step are determined and the census particle list is converted to numeric weights in order to form the initial condition for the transport equation during the next time step.

4. Discretization of the material state variable

In our piecewise linear Symbolic Implicit Monte Carlo solution of the difference formulation, we use piecewise linear basis functions to handle the spatial discretization of the material state variable. The spatial basis functions, permitting discontinuity at zone boundaries, are the same as those that were employed by Clouet and Samba [7] in their linearized treatment of the transport equation. Later on in our discussion, we will describe how to constrain the solution of the material energy equation so that continuity is preserved at interfaces between interior zones. This is appropriate when the physical properties of the material do not undergo significant change when crossing the interface.

We write out the linear basis functions, supporting discontinuities at zone edges, in slab geometry, in order to establish our notation. Extension to two and three dimensional geometry was described by Clouet and Samba, but will not be discussed here.

We define N zones, Z_i, $i \in (1, N)$. In each zone there are L basis functions, χ_i^l, $l \in (1, L)$. In slab geometry, $L = 2$. Denoting the left and right boundaries of Z_i by x_i and x_{i+1} respectively, the basis functions for slab geometry are defined as

$$\chi_i^1(x) = \begin{cases} 0 & (x < x_i), \\ \frac{x_{i+1}-x}{x_{i+1}-x_i} & (x_i \leqslant x < x_{i+1}), \\ 0 & (x_{i+1} \leqslant x), \end{cases} \tag{7}$$

$$\chi_i^2(x) = \begin{cases} 0 & (x < x_i), \\ \frac{x-x_i}{x_{i+1}-x_i} & (x_i \leqslant x < x_{i+1}), \\ 0 & (x_{i+1} \leqslant x). \end{cases} \tag{8}$$

It is easy to see that

$$\sum_{l=1}^{L} \chi_i^l(x) = 1 \quad (x_i \leqslant x < x_{i+1}) \tag{9}$$

and is zero otherwise. The fact that the basis functions add up to one within each zone makes it easy to assure energy conservation, and can be exploited when sampling [7] although we do not do so.

Defining

$$\overline{\chi_i^l}(x) = (2/(x_{i+1} - x_i))\chi_i^l(x), \tag{10}$$

we produce a normalized basis function with unit integral. This version of the basis function is useful when decomposing source terms for the purpose of Monte Carlo sampling. The concept will be extended to cover products of basis functions later on.

It is sometimes useful to organize things in terms of the zone edges, x_i, $i \in (1, N+1)$, which are located at the left and right edges of the zones, Z_i, $i \in (1, N)$. We will be careful to point out when we do so.

Any piecewise linear function, $F(x,t)$, can be represented in terms of the spatial basis functions, $\chi_i^l(x)$, with the expansion

$$F(x,t) = \sum_{i=1}^{N} F_i(x,t) = \sum_{i=1}^{N} \sum_{l=1}^{L} F_i^l(x,t) = \sum_{i=1}^{N} \sum_{l=1}^{L} f_i^l(t)\chi_i^l(x). \tag{11}$$

The expansion permits discontinuity in $F(x)$ at the internal interfaces between zones as there is no constraint relating f_i^2 and f_{i+1}^1. If $F(x)$ is continuous on the zone boundaries, $f_i^2 = f_{i+1}^1$. Without any constraint of continuity at zone boundaries, this expansion form is referred to as linear-discontinuous in some of the finite element literature dealing with discrete ordinates transport.

In Eq. (11) we defined the spatial discretization method that we employ for the material state variable and, therefore, for the transport source terms. The time step is the interval between t_0 and $t_0 + \Delta t$. The temporal discretization determines the time dependence of the expansion coefficients, $f_i^l(t)$. We employ an implicit, backward-Euler, discretization for the expansion coefficients in order to obtain apparent unconditional stability for the time evolution, and correct coupling between the radiation field and the material temperature in the

diffusion limit [6]. The consequence of this choice is that a non-linear system must be solved for the unknown values of the expansion coefficients at the end of the time step.

5. The solution of the transport equation

We employ the Symbolic Implicit Monte Carlo (SIMC) technique [3] to produce a statistical sample of the solution to the transport equation that depends upon the unknown coefficients in the expansion of the material state variable at the end of the time step. Either a finite element expansion for the material temperature, $T(x,t)$, or for the black body radiation energy density at the material temperature, $\Phi(x,t) = aT^4$, can be used to construct the source terms of the transport equation. In either case, the sources are sampled statistically as Monte Carlo particles and Eq. (1) is solved by propagating the particles.

As shown in Eq. (6), the source terms for the transport equation can be factored using the chain rule, cleanly separating the frequency dependence from the strength of the sources. We would like to note that it is important to factor out the frequency dependence before decomposing the strength terms for the purpose of Monte Carlo sampling. By doing this, all particles born at a given space and time point can be sampled from the same frequency distribution.

Important assumptions of the scheme are that: the frequency distribution of thermally emitted photons, the absorption coefficients of photons as they traverse the time step, and any scattering coefficients, are all functions of space that are determined from information known at the beginning of the time step. We would like to note that stimulated (e.g. Compton) scattering is not consistent with these assumptions, with enhancements of the scattering coefficient being dependent upon the strength of the radiation field in the direction and frequency being scattered into. One must face this issue when considering practical applications of our method, but we ignore it for now.

In addition to the "symbolic" source terms in the transport equation, there are the initial conditions for each time step (the census photons left from the previous time step), and the possibility of prescribed sources of Monte Carlo particles from the boundary conditions. Unlike the sources associated with the $\partial B/\partial t$ and $\partial B/\partial x$ terms in Eq. (6), these sources have numeric weights without unknown factors. Using these sources, the exact initial and boundary conditions for the transport problem are rigorously satisfied.

6. Monte Carlo sampling the source terms

In extending the Symbolic Implicit Monte Carlo method to a finite element treatment of the material energy equation, we are free to choose between expanding $\Phi(x,t) = aT^4$ or the material temperature, $T(x,t)$, in the basis functions. Examining Eq. (6), the advantage of expanding Φ becomes clear. With this choice the source terms are linear in Φ and this greatly simplifies the task of Monte Carlo sampling. It also makes the radiative coupling between zones linear. The disadvantage of expanding Φ, even for a constant material specific heat, is that the expression for the material energy is made non-linear. This problem becomes significant when one needs to lump the material energy in order to prevent negative excursions of the material state variable in the presence of steep gradients.

The alternative, expanding the material temperature, $T(x,t)$, in the linear basis functions, has its own advantages and disadvantages. The treatment of the material energy becomes linear, enabling lumping and straightforward coupling to other physics that treats the material temperature similarly. On the other hand, Monte Carlo sampling of the source terms is more complicated and the radiative coupling between zones becomes non-linear. We explore both approaches in our investigation, evaluating each one on its merits.

6.1. Expanding Φ in the finite element basis functions

Expanding $\Phi(x,t) = aT^4$ in the basis functions provides the simplest Monte Carlo implementation of the source terms:

$$\Phi(x,t) = \sum_{i=1}^{N} \Phi_i(x,t) = \sum_{i=1}^{N} \sum_{l=1}^{L} \Phi_i^l(x,t) = \sum_{i=1}^{N} \sum_{l=1}^{L} \phi_i^l(t)\chi_i^l(x). \tag{12}$$

In our detailed exposition of the Monte Carlo sampling of the source terms we assume the piecewise constant (in time) implicit temporal discretization described in Section 4 where the $\phi_i^l(t)$ abruptly jump to their end of time step values, $\phi_i^l(t_0+\Delta t)$, immediately after the beginning of the time step.

We now use the spatial expansion of Φ defined in Eq. (12), the definition of the strength of the source terms from Eq. (6) after factoring out the frequency distribution function given by $(4\pi/c)(\partial B/\partial\Phi)$, and the above understanding of the temporal treatment, to write down the source terms for the Monte Carlo treatment. First, we write the strength of the time derivative source from Eq. (6) in terms of normalized functions for the generalized particle coordinates, for the purpose of defining a sampling scheme. In the last manipulation we use the definition of the normalized basis function defined in Eq. (10):

$$-\frac{1}{4\pi}\frac{\partial\Phi_i(x,t)}{\partial t} = -\frac{1}{4\pi}\sum_l \frac{\mathrm{d}\phi_i^l(t)}{\mathrm{d}t}\chi_i^l(x) = -\frac{1}{4\pi}\sum_l \delta(t-t_0)(\phi_i^l(t_0+\Delta t)-\phi_i^l(t_0))\chi_i^l(x)$$
$$= -\frac{x_{i+1}-x_i}{[2]\times 4\pi}\sum_l [\delta(t-t_0)](\phi_i^l(t_0+\Delta t)-\phi_i^l(t_0))[\overline{\chi_i^l}(x)]. \tag{13}$$

The distribution functions for generalized particle coordinates have been denoted by enclosure in [ ]. The angular distribution function, 1/2, which provides for a uniform distribution for μ in the range $[-1,1]$, is included in the denominator, 8π. There are two spatial distributions for particles born in zone Z_i: those distributed according to $\overline{\chi_i^1}(x)$ and those distributed according to $\overline{\chi_i^2}(x)$. The temporal distribution function is $\delta(t-t_0)$, where δ is the Dirac delta function, indicating that all source particles are born at the beginning of the time step. In our implementation we emit two equally sized samples of M particles in each zone, spatially distributed according to $\overline{\chi_i^l}(x)$ and having a numeric weight $-(x_{i+1}-x_i)/(4\pi M)$. Each particle carries an unknown factor, $(\phi_i^l(t_0+\Delta t)-\phi_i^l(t_0))$, arising from the fact that $\phi_i^l(t_0+\Delta t)$ is not yet known. The variable M is a parameter controlling the sample count, and therefore the level of Monte Carlo noise appearing in the calculation.

The final detail is the frequency distribution for the source particles. As the frequency distribution must be determined before we know $\phi_i^l(t_0+\Delta t)$, we use values extrapolated from past behavior $\widetilde{\phi}_i^l(t_0+\Delta t)$ as a substitute for this purpose. This is a simple linear extrapolation from the prior time step. The frequency distribution is the finite difference form of $(4\pi/c)(\partial B/\partial\Phi)$ using $\Phi(x,t_0)$ and $\widetilde{\Phi}(x,t_0+\Delta t)$ evaluated at the point, x, sampled for each particle.

Lacking any constraint enforcing continuity of $\Phi(x,t)$ at the interior zone edges, x_i, $i\in(2,N)$, there are two components associated with the $\partial B/\partial x$ source term defined in Eq. (6). The first is a source of particles emitted *within* zone Z_i, again using the implicit time treatment discussed in Section 4,

$$-\frac{\mu c}{4\pi}\frac{\partial\Phi_i(x,t)}{\partial x} = -\frac{\mu c}{4\pi}\sum_l \phi_i^l(t)\frac{\mathrm{d}\chi_i^l(x)}{\mathrm{d}x} = -\frac{\mu c}{4\pi}\frac{\phi_i^2(t)-\phi_i^1(t)}{x_{i+1}-x_i} = -\frac{\mu c}{4\pi}\frac{(\phi_i^2(t_0+\Delta t)-\phi_i^1(t_0+\Delta t))}{x_{i+1}-x_i}$$
$$= -\frac{[2\mu]c\Delta t}{8\pi}\frac{(\phi_i^2(t_0+\Delta t)-\phi_i^1(t_0+\Delta t))}{[\Delta t][x_{i+1}-x_i]}. \tag{14}$$

As was discussed in [2], the integral of this source over the range of μ is zero. We deal with this by sampling the range of μ from 0 to 1 and emitting a pair of particles of equal and opposite weight and direction. With that understood, we can read off the distribution functions that have been denoted by enclosure in [ ]. The distribution function for μ is 2μ. The distribution function for the time coordinate is $1/\Delta t$, reflecting a uniform distribution across the interval from t_0 to $t_0+\Delta t$. The spatial distribution function is $1/(x_{i+1}-x_i)$, reflecting a uniform distribution across zone Z_i. M particle pairs are emitted within each zone, one member of each pair with a numeric weight of $-c\Delta t/8\pi M$ traveling in the positive μ direction, and the other with a weight of opposite sign traveling in the $-\mu$ direction. The particles carry the unknown factor $(\phi_i^2(t_0+\Delta t)-\phi_i^1(t_0+\Delta t))$. The frequency of the emitted particles is sampled using the frequency distribution $(4\pi/c)(\partial B/\partial\Phi)$ evaluated using $\Phi(x,t_0)$ at the position sampled.

The second component of the $\partial B/\partial x$ source term arises due to the possibility of a discontinuity of $\Phi(x,t)$ at the zone edges, x_i, $i\in(1,N+1)$. This singular contribution to the $\partial B/\partial x$ source term is

$$-\frac{\mu c}{4\pi}\delta(x-x_i)(\phi_i^1(t_0+\Delta t)-\phi_{i-1}^2(t_0+\Delta t)) = -\frac{[2\mu]c\Delta t}{8\pi[\Delta t]}[\delta(x-x_i)](\phi_i^1(t_0+\Delta t)-\phi_{i-1}^2(t_0+\Delta t)). \tag{15}$$

As was the case for the continuous $\partial B/\partial x$ source, this source is handled with correlated particle pairs of equal and opposite weight and direction, with the positive μ particle being distributed according to 2μ. The distribution function for the time coordinate is $1/\Delta t$. The spatial distribution function is $\delta(x - x_i)$, where x_i is the location of the interface between zones, or an exterior zone with a problem boundary. The values, ϕ_0^2 and ϕ_{N+1}^1, where N is the number of zones, refer to the boundary conditions for the left and right hand side of the problem, respectively. In this case we are dealing with a source arising from a discontinuity and the frequency of the emitted particles is sampled using the finite difference form of the frequency distribution $(4\pi/c)(\partial B/\partial \Phi)$, using $\Phi(x, t_0)$ on each side of the interface being sampled. There are $N + 1$ zone boundaries that contribute this source term.

6.2. Expanding T in the finite element basis functions

An alternative choice for handling the source terms is to expand the material temperature, T, in the finite element basis functions:

$$T(x,t) = \sum_{i=1}^{N} T_i(x,t) = \sum_{i=1}^{N}\sum_{l=1}^{L} T_i^l(x,t) = \sum_{i=1}^{N}\sum_{l=1}^{L} T_i^l(t)\chi_i^l(x). \tag{16}$$

This choice for the finite element expansion has the advantage that the material energy, assuming a constant specific heat during the time step, is linear. It is also likely that a second order accurate spatial treatment of other physics, such as hydrodynamics, would be more easily coupled to our transport method if this choice for the expansion of the material temperature is used. The disadvantages are the complexity of sampling the radiation source strength that scales like T^4, and the resulting non-linear radiative coupling between zones. This will become clear in what follows.

Using the definition, $\Phi = aT^4$, and the expansion for the temperature in zone Z_i given by Eq. (16), we rewrite the source terms defined in Eq. (6), within zone Z_i, again with the frequency dependence factored out:

$$-\frac{a}{4\pi}\frac{\partial (T_i(x,t))^4}{\partial t} = -\frac{a}{4\pi}\frac{\partial}{\partial t}\left(\sum_{l=1}^{L} T_i^l(t)\chi_i^l(x)\right)^4 = -\frac{a}{4\pi}\frac{\partial}{\partial t}(T_1^4\chi_1^4 + 4T_1^3T_2\chi_1^3\chi_2 + 6T_1^2T_2^2\chi_1^2\chi_2^2 + 4T_1T_2^3\chi_1\chi_2^3 + T_2^4\chi_2^4). \tag{17}$$

In writing the last form of Eq. (17), we have suppressed the zone index, i, and have moved the basis function index, l, to a subscript position in order to make it less cumbersome to write the powers of the temperatures and the basis functions. This notation will also be used in Appendix A.

As we did when expanding Φ in the basis functions, we use an implicit temporal treatment of the source terms. The time dependent coefficients jump from their value during the previous time step, $T(t_0)$, to their end of time step value, $T(t_0 + \Delta t)$, right at the beginning of the time step, leading to a Dirac delta function for the time derivative. Under this condition, Eq. (17) becomes

$$\begin{aligned}-\frac{a}{4\pi}\frac{\partial (T_i(x,t))^4}{\partial t} = -\frac{a}{4\pi}\delta(t-t_0)\{&(T_1^4(t_0+\Delta t) - T_1^4(t_0))\chi_1^4 + 4(T_1^3(t_0+\Delta t)T_2(t_0+\Delta t) - T_1^3(t_0)T_2(t_0))\chi_1^3\chi_2 \\ &+ 6(T_1^2(t_0+\Delta t)T_2^2(t_0+\Delta t) - T_1^2(t_0)T_2^2(t_0))\chi_1^2\chi_2^2 + 4(T_1(t_0+\Delta t)T_2^3(t_0+\Delta t) \\ &- T_1(t_0)T_2^3(t_0))\chi_1\chi_2^3 + (T_2^4(t_0+\Delta t) - T_2^4(t_0))\chi_2^4\}.\end{aligned} \tag{18}$$

Generalizing the notion expressed in Eq. (10), we rewrite Eq. (18) in terms of the normalized functions

$$\begin{aligned}\chi_1^4 &= \frac{\Delta x}{5}\overline{\chi_1^4}, \\ \chi_1^3\chi_2 &= \frac{\Delta x}{20}\overline{\chi_1^3\chi_2}, \\ \chi_1^2\chi_2^2 &= \frac{\Delta x}{30}\overline{\chi_1^2\chi_2^2}, \\ \chi_1\chi_2^3 &= \frac{\Delta x}{20}\overline{\chi_1\chi_2^3}, \\ \chi_2^4 &= \frac{\Delta x}{5}\overline{\chi_2^4},\end{aligned} \tag{19}$$

where Δx is the width of the zone. The result is

$$-\frac{a}{4\pi}\frac{\partial(T_i(x,t))^4}{\partial t} = -\frac{a\Delta x}{[2]\times 10\pi}[\delta(t-t_0)]\Big\{(T_1^4(t_0+\Delta t)-T_1^4(t_0))[\overline{\chi_1^4}] + (T_1^3(t_0+\Delta t)T_2(t_0+\Delta t) - T_1^3(t_0)T_2(t_0))[\overline{\chi_1^3\chi_2}] + (T_1^2(t_0+\Delta t)T_2^2(t_0+\Delta t) - T_1^2(t_0)T_2^2(t_0))[\overline{\chi_1^2\chi_2^2}] + (T_1(t_0+\Delta t)T_2^3(t_0+\Delta t) - T_1(t_0)T_2^3(t_0))[\overline{\chi_1\chi_2^3}] + (T_2^4(t_0+\Delta t)-T_2^4(t_0))[\overline{\chi_2^4}]\Big\}. \quad (20)$$

We can now read off how to sample this source term. This source is uniform in μ, reflected in the distribution function, 1/2, in the denominator, 20π. The temporal distribution function is $\delta(t-t_0)$, indicating that all of the source particles are born at the beginning of the time step. The numerical weight to be distributed among M sets of five particles is $-(a\Delta x)/(10\pi)$, with each member of a set of five particles receiving the weight $-(a\Delta x)/(10\pi M)$. Table 1 shows the unique characteristics of the members of a set of particles, namely their respective spatial distribution functions and unknown factors.

As was the case in our discussion of the source terms for linear Φ in a zone, the frequency dependence of the source term is factored using the chain rule before we decompose the strength of the source in terms of the spatial basis functions. The frequency distribution of the sampled particles is obtained from the finite difference form of $(4\pi/c)(\partial B/\partial\Phi)$, evaluated using the known temperature for the beginning of the time step, and the extrapolated temperature for the end of the time step, at the spatial position that was sampled for the particle. The details of sampling spatial positions within a zone, and sampling the frequency for a particle, are described in the appendix.

The continuous contribution to the $\partial B/\partial x$ source from Eq. (6), in terms of the piecewise linear treatment of the temperature in a zone, is given by

$$-\frac{\mu ca}{4\pi}\frac{\partial(T_i(x,t))^4}{\partial x} = -\frac{\mu ca}{4\pi}\frac{\partial}{\partial x}\left(\sum_{l=1}^{L}T_i^l(t)\chi_i^l(x)\right)^4 = -\frac{\mu ca}{\pi}\left(\sum_{l=1}^{L}T_i^l(t)\chi_i^l(x)\right)^3\frac{\partial}{\partial x}\left(\sum_{l=1}^{L}T_i^l(t)\chi_i^l(x)\right). \quad (21)$$

In our implicit temporal treatment, $T_i^l(t)$ during the time step is $T_i^l(t_0+\Delta t)$. The space derivative of $\chi_i^2(x)$, within zone Z_i, is $1/(x_{i+1}-x_i)$. The space derivative of $\chi_i^1(x)$ has the opposite sign. This provides

$$-\frac{\mu ca}{\pi(x_{i+1}-x_i)}\left(\sum_{l=1}^{L}T_i^l(t_0+\Delta t)\chi_i^l(x)\right)^3\left(T_i^2(t_0+\Delta t)-T_i^1(t_0+\Delta t)\right). \quad (22)$$

Again, suppressing the index i with the understanding that we are dealing with values associated with zone Z_i, moving the l index to a subscript position to avoid confusion with powers of the expansion coefficients for the temperature, and remembering that all temperature values are evaluated at the end of the time step, $(t_0+\Delta t)$, we expand the sum,

$$-\frac{\mu ca}{\pi\Delta x}\left(T_1^3\chi_1^3 + 3T_1^2T_2\chi_1^2\chi_2 + 3T_1T_2^2\chi_1\chi_2^2 + T_2^3\chi_2^3\right)(T_2-T_1), \quad (23)$$

where Δx is the width of the zone.

Table 1
A bundle of particles for the time derivative source terms in the expansion of T

Particle	Distribution	Unknown factor
1	$\overline{\chi_1^4}$	$(T_1^4(t_0+\Delta t)-T_1^4(t_0))$
2	$\overline{\chi_1^3\chi_2}$	$(T_1^3(t_0+\Delta t)T_2(t_0+\Delta t)-T_1^3(t_0)T_2(t_0))$
3	$\overline{\chi_1^2\chi_2^2}$	$(T_1^2(t_0+\Delta t)T_2^2(t_0+\Delta t)-T_1^2(t_0)T_2^2(t_0))$
4	$\overline{\chi_1^1\chi_2^3}$	$(T_1(t_0+\Delta t)T_2^3(t_0+\Delta t)-T_1(t_0)T_2^3(t_0))$
5	$\overline{\chi_2^4}$	$(T_2^4(t_0+\Delta t)-T_2^4(t_0))$

Each member of the set of five particles has a unique spatial distribution functions and an associated unknown factor.

Writing Eq. (23) in terms of the normalized functions

$$\begin{aligned}
\chi_1^3 &= \frac{\Delta x}{4}\overline{\chi_1^3},\\
\chi_1^2\chi_2 &= \frac{\Delta x}{12}\overline{\chi_1^2\chi_2},\\
\chi_1\chi_2^2 &= \frac{\Delta x}{12}\overline{\chi_1\chi_2^2},\\
\chi_2^3 &= \frac{\Delta x}{4}\overline{\chi_2^3}
\end{aligned} \tag{24}$$

and the distribution functions for the angular and time coordinates, we obtain

$$-\frac{[2\mu]ca\Delta t}{8\pi[\Delta t]}\left(T_1^3[\overline{\chi_1^3}] + T_1^2T_2[\overline{\chi_1^2\chi_2}] + T_1T_2^2[\overline{\chi_1\chi_2^2}] + T_2^3[\overline{\chi_2^3}]\right)(T_2 - T_1). \tag{25}$$

At this point, we can read off the sampling scheme for the Monte Carlo treatment of this source term. The angular distribution function is 2μ. As was the case for our piecewise linear treatment of Φ, we assure that the total source integrated over the range of μ is zero by sampling correlated particle pairs with equal and opposite weights in the $\pm\mu$ directions. In our Monte Carlo treatment of this source term, M sets of four particle pairs are created for each zone. The position coordinates for each of the four pairs in a set are sampled from $\{\overline{\chi_1^3}, \overline{\chi_1^2\chi_2}, \overline{\chi_1\chi_2^2}, \overline{\chi_2^3}\}$, and carry the unknown factors, $\{T_1^3(T_2 - T_1), T_1^2T_2(T_2 - T_1), T_1T_2^2(T_2 - T_1), T_2^3(T_2 - T_1)\}$, respectively. For a given pair, the particle sampled in the $+\mu$ direction has the numeric weight $-ca/8\pi M$, while the particle in the $-\mu$ direction has the opposite sign. The frequency distribution is $(4\pi/c)(\partial B/\partial\Phi)$ evaluated at the spatial point sampled.

If there is a discontinuity in $T(x,t)$ at the zone edges, x_i, $i \in (1, N+1)$, the space derivative source in Eq. (6) has a singular contribution, again with the frequency dependence factored out, given by

$$-\frac{\mu ca}{4\pi}\delta(x - x_i)\left((T_i^1(t))^4 - (T_{i-1}^2(t))^4\right), \quad i \in (1, N+1), \tag{26}$$

where $T_0^2(t)$ is the boundary condition on the left surface of the slab, and $T_{N+1}^1(t)$ is the boundary condition on the right and $\delta(x - x_i)$ is a Dirac delta function. Identifying the angular, temporal and spatial distribution functions, and with our implicit differencing scheme that evaluates the temperatures at the end of time step values, the singular contribution to the $\partial B/\partial x$ source term becomes

$$-\frac{[2\mu]ca\Delta t}{8\pi[\Delta t]}\delta(x - x_i)\left((T_i^1)^4 - (T_{i-1}^2)^4\right), \quad i \in (1, N+1), \tag{27}$$

where 2μ is the angular distribution function for the $+\mu$ particle of a $\pm\mu$ particle pair, $1/\Delta t$ is the distribution function for particles uniformly distributed across the time step, and $\delta(x - x_i)$ is the spatial distribution function indicating that the particle pairs are born on the zone interface, located at x_i. If M particle pairs are sampled at each interface, the ones traveling in the $+\mu$ direction have a numeric weight of $-ca\Delta t/8\pi M$ and carry the unknown factor $((T_i^1)^4 - (T_{i-1}^2)^4)$, the difference in the fourth power of the temperature on each side of the interface. The frequency for the particles is sampled using the finite difference form of $(4\pi/c)(\partial B/\partial\Phi)$, evaluated using $\Phi(x, t_0)$ on each side of the interface.

7. Galerkin treatment of the material energy equation

In the prior section, we described how to deal with source particle sampling in the presence of unknown coefficients, whether they be the $\phi_i^l(t_0 + \Delta t)$ in the case of linear treatment of Φ in a zone (as a function of space), or the $T_i^l(t_0 + \Delta t)$ in the case of linear treatment of T in a zone. Using the basis function representation of the source terms, correct spatial distributions can be established for Monte Carlo source particles whose weights have not yet been determined.

We must solve the material energy equation, Eq. (2), in order to determine the unknown coefficients of the expansion of Φ, or T, at the end of the time step. The method of solving the material energy equation determines how we score energy deposition of the particles that get tracked in our Monte Carlo treatment of the

transport equation, Eq. (1). To this end, we formally integrate the material energy equation from t_0 to $t_0 + \Delta t$, bring the change in material energy to the right hand side, and refer to the result as the non-linear function $F(x)$, which must equal zero. The $F(x)$, here, is not to be confused with Eq. (11):

$$F(x) = E_{\mathrm{mat}}(T(x,t_0)) - E_{\mathrm{mat}}(T(x,t_0+\Delta t)) + 2\pi \int_{t_0}^{t_0+\Delta t} \mathrm{d}t \int_0^{\infty} \mathrm{d}v \int_{-1}^{1} \mathrm{d}\mu \sigma'_a(v, T(x,t_0)) D(x,t;v;\mu) + \int_{t_0}^{t_0+\Delta t} \mathrm{d}t G(x,t). \tag{28}$$

We would like to note that we are using $\sigma'_a(v, T(x,t_0))$, the opacity at the beginning of the time step, for the time integral of the difference field. In order to run the Monte Carlo solution to the transport equation, any absorption and scattering cross sections must be evaluated using temperatures from the beginning of the time step, $T(x,t_0)$.

$F(x)$ is a non-linear function of the $\phi_i^l(t_0+\Delta t)$, or the $T_i^l(t_0+\Delta t)$, as the case may be. If the unknown coefficients are the $\phi_i^l(t_0+\Delta t)$, the non-linearity occurs in the expression of the material energy. If the coefficients of the expansion are the $T_i^l(t_0+\Delta t)$, the non-linearity occurs in the unknown factors in the time integral of $\sigma'_a D$. The local heating rate, G, is prescribed.

Generally, the function $F(x)$ is also a non-linear function of the position coordinate, x. Because of this we pursue a Galerkin treatment for the solution of $F(x) = 0$; we generate a set of algebraic equations to solve for the expansion coefficients, $\phi_i^l(t_0+\Delta t)$ or $T_i^l(t_0+\Delta t)$ as the case may be, by requiring that the projection of $F(x)$ onto the basis functions $\chi_j^k(x)$ defined by,

$$F_j^k = \int \mathrm{d}x \chi_j^k(x) F(x), \tag{29}$$

be zero.

Identifying the terms in $F(x)$ from Eq. (28), we define

$$E_j^k(t) = \int \mathrm{d}x \chi_j^k(x) E_{\mathrm{mat}}(x,t), \tag{30}$$

$$(\sigma D)_j^k = 2\pi \int \mathrm{d}x \chi_j^k(x) \int_{t_0}^{t_0+\Delta t} \mathrm{d}t \int_0^{\infty} \mathrm{d}v \int_{-1}^{1} \mathrm{d}\mu \sigma'_a(v, T(x,t_0)) D(x,t;v;\mu) \tag{31}$$

and

$$G_j^k = \int \mathrm{d}x \int_{t_0}^{t_0+\Delta t} \mathrm{d}t \chi_j^k(x) G(x,t). \tag{32}$$

In terms of these definitions, we can write the algebraic system of equations we must solve as

$$F_j^k = E_j^k(t_0) - E_j^k(t_0+\Delta t) + (\sigma D)_j^k + G_j^k = 0. \tag{33}$$

The projection of the material energy at the start of the time step, $E_j^k(t_0)$, depends only upon known variables. The projection of the heat source during the time step, G_j^k, is prescribed. The projection of the material energy at the end of the time step, $E_j^k(t_0+\Delta t)$, is non-linear when expressed in terms of the $\phi_i^l(t_0+\Delta t)$ and linear when expressed in terms of the $T_i^l(t_0+\Delta t)$. Additionally, it depends only upon the coefficients for basis functions in the same zone. The projection of the energy deposited from photon transport, $(\sigma D)_j^k$, is linear if the source terms are expressed in terms of the $\phi_i^l(t_0+\Delta t)$ and non-linear when the source terms are expressed in terms of the $T_i^l(t_0+\Delta t)$. It also has a component that comes from the census particles from the prior time step that can be considered an initial condition for the difference field at the start of the time step.

As noted above, and further exposited below, the system of algebraic equations, $F_j^k = 0$, is non-linear in its unknowns and we employ Newton–Raphson iteration for the solution. We start with a guess for the solution, the value of the dependent variables at the beginning of the time step, or some extrapolated value, and evaluate both F_j^k and the partial derivatives of F_j^k with respect to the unknowns at this starting point. We then solve a linear system for the error, producing a new value for the solution. This process is iterated until convergence is achieved. Our solution strategy, then, boils down to evaluating the projection of the material

energy at the end of the time step, $E_j^k(t_0+\Delta t)$, the projection of the absorbed energy, $(\sigma D)_j^k$, and their derivatives with respect to the unknown variables at the trial values for the solution, and then refining them using Newton–Raphson iteration.

We start with the material energy in terms of the ϕ_i^l. Inverting $\Phi = aT^4$, we have $T = \Phi^{1/4}/a^{1/4}$. The energy density of the material, assuming a constant specific heat, c_v, and a constant material density, ρ, is

$$E(\Phi(x)) = \frac{\rho c_v}{a^{1/4}}\Phi^{1/4}(x). \tag{34}$$

In zone Z_i, $\Phi(x,t)$ is given by

$$\Phi_i(x,t) = \phi_i^1(t)\chi_i^1(x) + \phi_i^2(t)\chi_i^2(x). \tag{35}$$

The material energy density within the zone, then, is

$$E_i(x,t) = \frac{\rho c_v}{a^{1/4}}\left(\phi_i^1(t)\chi_i^1(x) + \phi_i^2(t)\chi_i^2(x)\right)^{1/4} \tag{36}$$

and the total material energy is

$$E(x,t) = \sum_i E_i(x,t). \tag{37}$$

The projection of the material energy, defined above, is

$$E_j^k(t) = \int \mathrm{d}x\chi_j^k(x)E(x,t) = \int \mathrm{d}x\chi_j^k(x)E_j(x,t), \tag{38}$$

where the basis function χ_j^k selects $i=j$.

We find that the E_j^k may be evaluated, in terms of $\phi_j^1(t)$ and $\phi_j^2(t)$, in closed form using a symbolic manipulation package such as Mathematica,

$$\begin{aligned} E_j^1(t) = \frac{\rho c_v}{a^{1/4}}4\Delta x(&5\phi_1^{7/4} + 10\phi_1^{3/2}\phi_2^{1/4} + 15\phi_1^{5/4}\phi_2^{1/2} + 20\phi_1\phi_2^{3/4} + 16\phi_1^{3/4}\phi_2 + 12\phi_1^{1/2}\phi_2^{5/4} + 8\phi_1^{1/4}\phi_2^{3/2} \\ &+ 4\phi_2^{7/4})/(45(\phi_1^{1/4}+\phi_2^{1/4})^2(\phi_1^{1/2}+\phi_2^{1/2})^2), \end{aligned} \tag{39}$$

where Δx is the width of zone j. We have suppressed the common subscript, j, on the right hand side, and have moved the basis function indices to the subscript in order to cleanly display the fractional powers. All of the ϕ are understood to be functions of time, t. $E_j^2(t)$ is obtained by symmetry.

For the Newton–Raphson iteration of the solution, we require the partial derivative of $E_j^1(t)$ with respect to ϕ_1 and ϕ_2. These, again, can be evaluated in closed form:

$$\begin{aligned} \frac{\partial E_j^1(t)}{\partial\phi_1} = \frac{\rho c_v}{a^{1/4}}\Delta x(&5\phi_1^{3/2} + 15\phi_1^{5/4}\phi_2^{1/4} + 30\phi_1\phi_2^{1/2} + 50\phi_1^{3/4}\phi_2^{3/4} \\ &+ 57\phi_1^{1/2}\phi_2 + 51\phi_1^{1/4}\phi_2^{5/4} + 32\phi_2^{3/2})/(45(\phi_1^{1/4}+\phi_2^{1/4})^3(\phi_1^{1/2}+\phi_2^{1/2})^3), \end{aligned} \tag{40}$$

$$\begin{aligned} \frac{\partial E_j^1(t)}{\partial\phi_2} = \frac{\rho c_v}{a^{1/4}}4\Delta x(&\phi_1^{3/2} + 3\phi_1^{5/4}\phi_2^{1/4} + 6\phi_1\phi_2^{1/2} + 10\phi_1^{3/4}\phi_2^{3/4} \\ &+ 6\phi_1^{1/2}\phi_2 + 3\phi_1^{1/4}\phi_2^{5/4} + \phi_2^{3/2})/(45(\phi_1^{1/4}+\phi_2^{1/4})^3(\phi_1^{1/2}+\phi_2^{1/2})^3), \end{aligned} \tag{41}$$

$$\frac{\partial E_j^2(t)}{\partial\phi_1} = \frac{\partial E_j^1(t)}{\partial\phi_2}, \tag{42}$$

$$\frac{\partial E_j^2(t)}{\partial\phi_2} = \frac{\partial E_j^1(t)}{\partial\phi_1}. \tag{43}$$

The non-linearity of the material energy when we expand Φ in the basis functions is clear.

At the cost of a non-linear treatment of the source terms for the difference field, we can have a linear treatment of the material energy. Again, assuming a constant specific heat, we have

$$E(T(x)) = \rho c_v T(x), \tag{44}$$

$$T_j(x,t) = T_j^1(t)\chi_j^1(x) + T_j^2(t)\chi_j^2(x) \tag{45}$$

and

$$E_j^1(t) = \rho c_v \Delta x \left(\frac{T_j^1(t)}{3} + \frac{T_j^2(t)}{6}\right), \tag{46}$$

where $E_j^2(t)$ is obtained by exchanging the basis function indices, 1 and 2, on the right hand side. Unlike the case for linear Φ, the linearity of the material energy expressed in terms of T allows one to cleanly separate the portion of the energy due to T_j^1 from the portion of the energy due to T_j^2. When the consistent projection of the material energy onto the χ_j^k generates trouble in the presence of steep gradients, we can lump the material energy on each end of the zone so that E_j^1 depends only upon T_j^1, and E_j^2 depends only upon T_j^2:

$$E_j^k(t)_{\text{lumped}} = \frac{\rho c_v \Delta x}{2} T_j^k(t). \tag{47}$$

This corresponds to adding the off-diagonal terms in the 2×2 matrix representing the heat capacity within a zone to the diagonal terms. This reduces the accuracy of the time dependent solution, but can be used to remove the monotonicity problem that would otherwise occur, thereby avoiding negative temperature solutions.

We are left with

$$(\sigma D)_j^k = 2\pi \int \mathrm{d}x \int_{t_0}^{t_0+\Delta t} \mathrm{d}t \int_0^\infty \mathrm{d}v \int_{-1}^{1} \mathrm{d}\mu \chi_j^k(x)\sigma_a'(v, T(x,t_0))D(x,t;v;\mu) \tag{48}$$

understanding that in addition to contributions from numeric (census) particles, contributions will come from symbolic particles carrying unknown factors involving $\phi_i^l(t_0+\Delta t)$, or $T_i^l(t_0+\Delta t)$. In the case of a constant $\sigma_a'(v, T(x,t_0))$, as a function of temperature, the contribution of a particle track to the $(\sigma D)_j^k$ can be evaluated in closed form. In the case of a temperature dependent opacity, one might have to execute a multi-step numerical integration along the track, or use the first few terms of a power series expansion.

Separating the energy depositions from the different particle types when we are expanding the source terms in terms of the ϕ_i^l, the projection of the energy deposition can be written as

$$\begin{aligned}(\sigma D)_j^k = {} & N_j^k + \sum_{i=1}^{N}\sum_{l=1}^{L}(DDT_i^l)_j^k(\phi_i^l(t_0) - \phi_i^l(t_0+\Delta t)) + \sum_{i=1}^{N}(DDX_i)_j^k(\phi_i^1(t_0+\Delta t) - \phi_i^2(t_0+\Delta t)) \\ & + \sum_{i=1}^{N+1}(DELTA_i)_j^k(\phi_{i-1}^2(t_0+\Delta t) - \phi_i^1(t_0+\Delta t)),\end{aligned} \tag{49}$$

where N_j^k is the contribution from census particles from the prior time step, $(DDT_i^l)_j^k$ is the contribution from $\partial/\partial t$ source particles born via $\overline{\chi_i^l}(x)$ in Eq. (13), $(DDX_i)_j^k$ is the contribution from $\partial/\partial x$ source particles born via Eq. (14), and $(DELTA_i)_j^k$ is the contribution from $\partial/\partial x$ source particles born via Eq. (15). In order to get the actual contribution to the energy deposition, these matrix elements must be multiplied by the appropriate unknown factors. The coefficients with out of range indices, $\phi_0^2(t_0+\Delta t)$ and $\phi_{N+1}^1(t_0+\Delta t)$, represent prescribed boundary conditions for the problem.

The structure of the energy deposition when expanding T in the finite element basis in order to generate the source terms can be similarly expressed in terms of 10 different particle types and appropriate unknown factors.

7.1. Scoring a particle track

The $D(x,t;v;\mu)$ associated with a Monte Carlo particle track is

$$cD_0 \mathrm{e}^{-\sigma_a'(v)c(t-t_0)}\delta(x - x_0 - \mu_0 c(t-t_0))\delta(v - v_0)\delta(\mu - \mu_0), \tag{50}$$

where D_0 is the weight of the particle at the start of the track and $(x_0, t_0; v_0; \mu_0)$ are the generalized coordinates of the particle at the start of the track, not the start of the time step. We are assuming, for the purpose of this

discussion, that the track is made entirely within zone Z_j and within the time step, and that $\sigma'_a(v,T)$ is independent of temperature. The discussion can be extended to cover the more complicated case.

The contribution of a particle track, defined in Eq. (50), to the term $(\sigma D)^k_j$, defined in Eq. (48), is calculated (modulo any unknown factor) by inserting the expression for the particle track into Eq. (48) and evaluating the integral. The integral over v selects $\sigma'_a(v_0)$ and the integral over μ drops out trivially. The remaining delta function, enclosed in the integral over x, converts the x in the basis function to $x_0+\mu_0 c(t-t_0)$, obtaining

$$\int_{t_0}^{t_0+t'} \mathrm{d}tc\sigma'_a(v_0)\chi^k_j(x_0+\mu_0 c(t-t_0))D_0 \mathrm{e}^{-\sigma'_a(v_0)c(t-t_0)} = \int_0^{t'} \mathrm{d}tc\sigma'_a(v_0)\chi^k_j(x_0+\mu_0 ct)D_0 \mathrm{e}^{-\sigma'_a(v_0)ct}. \tag{51}$$

For χ^1_j the result is

$$D_0 \frac{(\mu_0 + c\mu_0\sigma'_a(v_0)t + \sigma'_a(v_0)(x_0 - x_{i+1}))}{\sigma'_a(v_0)(x_{i+1}-x_i)} \mathrm{e}^{-\sigma'_a(v_0)ct}\Big|_0^{t'}. \tag{52}$$

For χ^2_j the result is

$$D_0 \frac{(\mu_0 + c\mu_0\sigma'_a(v_0)t + \sigma'_a(v_0)(x_0 - x_i))}{\sigma'_a(v_0)(x_{i+1}-x_i)} \mathrm{e}^{-\sigma'_a(v_0)ct}\Big|_{t'}^0. \tag{53}$$

The sum is

$$D_0 \mathrm{e}^{-\sigma'_a(v_0)ct}\Big|_{t'}^0, \tag{54}$$

this being the weight lost by the particle during the track. The weight, D_0, may contain an unknown factor, leading to scoring the track in the appropriate matrix element.

8. Numerical results with a piecewise linear Φ

In presenting numerical results employing the piecewise linear treatment of Φ, our goal is to demonstrate the lack of monotonicity that occurs in the presence of strong gradients and to demonstrate the advantage for this expansion choice near steady state. The basic test problem that we use for this demonstration is one where a finite slab is abruptly subjected to an incoming black body radiation flux on the left boundary while the right boundary radiates freely with no incoming radiation flux. Assuming that the incoming black body flux corresponds to a temperature higher than the initial material temperature, and with an initial radiation field that is in equilibrium with the material temperature, a thermal (Marshak) wave propagates from the left to the right. The material conditions eventually come to steady state and there is a steady energy flow through the material.

In Fig. 1 we show an early time result for such a problem. The grey opacity is one mean free path per cm and the specific heat of the material is given by $\rho c_v = 0.1$ jerk/cm^3 keV.[1] The initial temperature is $kT = 0.4$ keV and the slab is subjected to a $kT = 1$ keV black body applied on the left hand side at the start of the simulation. The time step size is 0.001 sh. With the dotted line, we show the material temperature at 0.03 sh using zones that are 1 cm thick, five zones for the problem. The solid line shows the 50 zone converged solution using the same computational method. The material temperature is discontinuous at zone boundaries, this being allowed by the finite element basis choice.

Two specific features of the five zone solution are notable. The first is that the curvature provided by the linear treatment of Φ is a poor fit for the leading edge of a Marshak wave, as demonstrated by comparison to the converged solution. The second is the relatively severe undershoot for the right side of the first zone, relative to the converged solution, occurring in spite of the fact that the energy deposited on this side of the zone is positive. This undershoot is a property of the finite zone size, not the finite time step size. It results from the self-consistent solution of the material energy equation given the lopsided energy deposition in the first zone. The existence of the undershoot prevents us from running with a zero initial material temperature. The nonlinearity of the material energy, when expressed in terms of Φ, makes it difficult to remove this pathology.

[1] Our units are 1 sh (shake) $= 10^{-8}$ s; temperature is measured in energy units, kT in keV; frequency is measured in energy units, $h\nu$ in keV; and the material energy is measured in jerks, 1 jerk $= 10^9$ J.

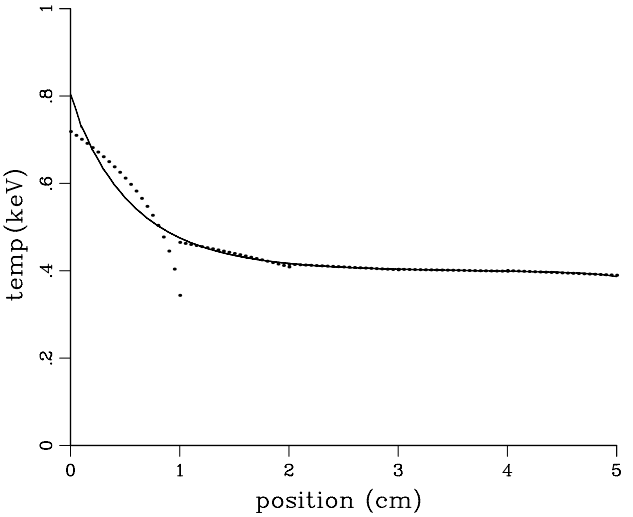

Fig. 1. A problem demonstrating the monotonicity issue, at a time $t = 0.03$ sh. The right hand side of the first zone has dropped below the initial temperature, $kT = 0.4$ keV, even though the energy deposited there has always been positive. The solid line shows the converged, 50 zone, solution. The dotted line shows the five zone solution. The solution for the temperature within the zone is curved because it is $\Phi = aT^4$ that is represented as a linear function within a zone.

Although the lack of monotonicity in the presence of steep gradients is a serious difficulty that limits the utility of this formulation, the linear treatment of Φ within a zone leads to a very accurate solution for problems near steady state where such steep gradients do not exist. In Fig. 2 we show the solution for the problem defined above at a late time near steady state, again comparing the five zone solution to the converged 50 zone solution. Only the boundary layer in the last centimeter at the right hand side of the 5 cm thick slab is shown; it has one zone for the five zone solution and 10 zones for the 50 zone solution. The treatment of the boundary layer is fully converged with the 50 zone solution. In the interior of the slab, the five zone solution is in complete agreement with the 50 zone solution, reflecting the accuracy of the linear treatment of Φ for these physical conditions. In the first mean free path on the left hand side of the slab there is another boundary layer, but this is not shown in figure.

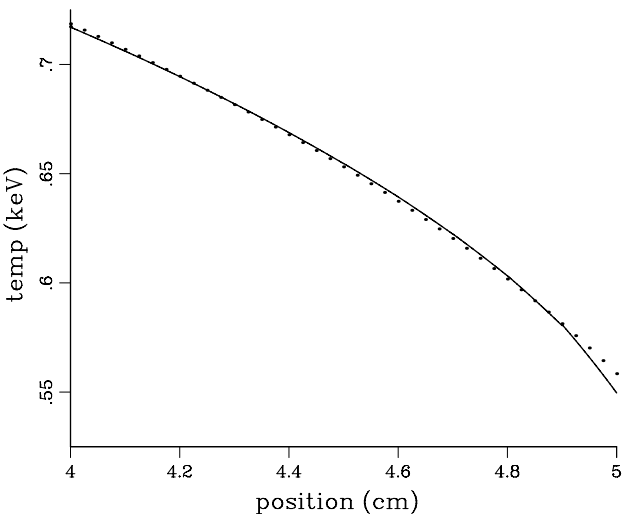

Fig. 2. The outer edge of the slab of the problem of Fig. 1, one mean free path thick, shown at a late time near steady state. For the five zone discretization, the span from 4 to 5 cm is represented with one zone. This result is shown in the dotted line. For the 50 zone discretization, the same span is 10 zones, shown in the solid line. The small difference is the influence of the boundary layer.

9. Numerical results with a piecewise linear T

Given the monotonicity issue that has surfaced, we will now focus on the development of the piecewise linear treatment of the material temperature, T, in our remaining exposition. First, we repeat the problems run in Figs. 1 and 2 so that we may compare, generally, the characteristics of the two choices for the material state variable, Φ and T. We will then show how lumping the material energy addresses the problem with monotonicity.

The results for the problem of Fig. 1, which uses the finite element expansion of Φ, are repeated using the finite element expansion of T in Fig. 3. Comparing Figs. 1 and 3, we see that the converged 50 zone result is identical, and that the linear treatment of T in a zone provides a better match when compared to the converged solution for the leading edge of the Marshak wave. The linear treatment of T in the zone also tends to produce less undershoot on the back side of a zone in the presence of a strong gradient, although an undershoot is still present and must be dealt with.

The results for the problem of Fig. 2, which uses an expansion of Φ in linear basis functions, are repeated using the linear expansion of T in Fig. 4. Comparing Figs. 2 and 4, we see that the linear treatment of Φ does better, compared to the linear treatment of T, with small zone counts near steady state conditions, although the second order accuracy provides for an accurate solution with only a modest increase in zone count.

The improved undershoot in the presence of strong gradients makes the linear treatment of T more robust for time dependent problems, but it still suffers from the monotonicity problem. These undershoots will cause a negative temperature if the initial temperature in front of an advancing Marshak wave is low enough. The linear treatment of the material energy makes it possible to lump the material energy, regaining monotonicity in the presence of a strong gradient.

In Fig. 5 we explore the effect of a lumped treatment of the material energy. We show the material temperature for the problem of Fig. 3, except that the initial temperature is reduced to 0.2 keV and the result is shown at a slightly later time of 0.035 sh, adding results for a lumped material energy with the dotted line. The discontinuous solid line is the result without lumping. The continuous solid line is the converged 50 zone solution. By lumping the material energy we make an error that causes the slope within a zone to be incorrect. In order to minimize any accumulated error due to lumping, we employ conditional lumping in problems we show later in this paper. In conditional lumping, we lump the material energy in a specific zone only during a time step where failing to lump would cause a negative temperature excursion.

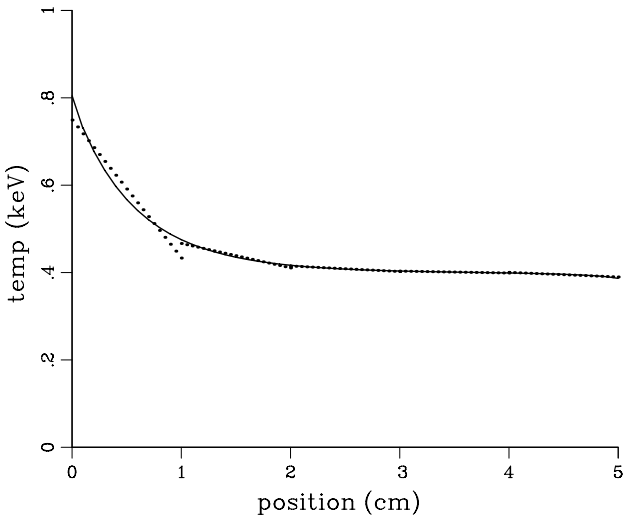

Fig. 3. A repeat of the calculation of Fig. 1 using a linear expansion of T for the source terms. The dotted line is the five zone solution. The continuous line is the converged 50 zone solution.

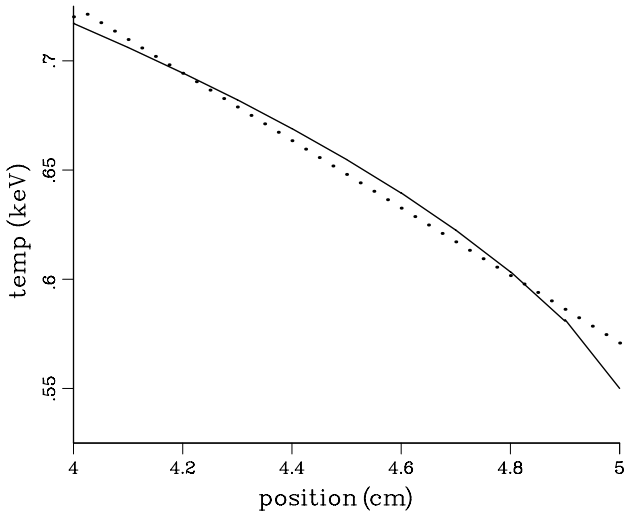

Fig. 4. A repeat of the calculation of Fig. 2 using a linear expansion of T for the source terms. The dotted line is the five zone solution, one zone in the centimeter span shown. The solid line is the converged 50 zone solution.

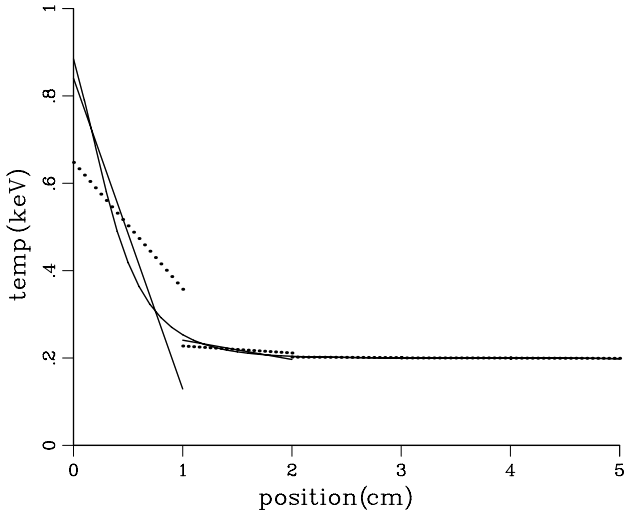

Fig. 5. A calculation showing the effect of continuous lumping. The time, $t = 0.035$ sh. The dotted line is for the five zone lumped case, with the discontinuous solid line not lumped. The solid continuous line is the converged 50 zone case.

10. Constraining the solution to be continuous

Our choice for the finite element basis expansion allows discontinuity in the material temperature at internal zone interfaces, a situation also referred to as linear-discontinuous in some of the finite element literature. The cost of allowing these discontinuities is that we must deal with $2N$ unknowns where N is the number of zones in our one dimensional slab geometry setting. This can substantially increase the cost of the non-linear system solve and allow any undershoot to be worse than would occur if the left and right hand temperatures of an internal zone interface were constrained to agree. In this section we discuss, briefly, how to produce the solution corresponding to a basis that enforces continuity on the zone interfaces internal to the problem domain. This procedure is useful when the opacity is not discontinuous at the interface between zones, and can be applied selectively.

A basis function set that provides for a single temperature at each internal zone interface can be defined as follows:

$$\begin{aligned}\psi_1(x) &= \chi_1^1(x),\\ \psi_i(x) &= \chi_{i-1}^2(x) + \chi_i^1(x) \quad (1 < i \leqslant N),\\ \psi_{N+1}(x) &= \chi_N^2(x).\end{aligned} \tag{55}$$

By expanding the material temperature in this basis, there are $N+1$ coefficients for the expansion, these being the values of the material temperature on the zone interfaces, both internal and external.

The projections of $F(x)$ defined by Eq. (28) on the ψ_j, F_j^ψ, can be obtained adding the appropriate F_j^k defined by Eq. (29):

$$\begin{aligned}F_1^\psi &= F_1^1,\\ F_i^\psi &= F_{i-1}^2 + F_i^1 \quad (1 < i \leqslant N),\\ F_{N+1}^\psi &= F_N^2.\end{aligned} \tag{56}$$

These projections are required for the Newton–Raphson solution of the non-linear system that represents the energy equation in terms of the ψ basis and are evaluated at the temperatures that are iterated to solution.

The partial derivatives of the F_j^ψ with respect to the unknown coefficients of the temperature expanded in the ψ_i basis, evaluated at the iterated zone edge temperatures, are also needed for the Newton–Raphson solution. These are obtained by adding the partial derivatives with respect to the coefficients of χ_{i-1}^2 and χ_i^1, evaluated at the temperature that is now shared between them.

The process collapses the $2N \times 2N$ Jacobian of the non-linear system in terms of the χ basis to a $(N+1)\times(N+1)$ Jacobian in terms of the ψ basis (for a 1-D problem), requiring only addition of matrix elements. This obtains the solution for the ψ basis with a relatively local modification of the code used to compute the solution in terms of the χ basis. In addition, the $\mathrm{d}B/\mathrm{d}x$ source particles associated with the discontinuities at interior zone interfaces that are not allowed with the ψ basis need not be emitted as their weights will always be zero. This leads to additional computational efficiency.

In Fig. 6 we overlay the results of this treatment with the prior results of Fig. 5. The undershoot at the right edge of the first zone is made less severe by the constraint of continuity, but this basis still suffers from the lack of monotonicity unless lumping is used in order to avoid it.

In Fig. 7 we show the temperature of the continuous solution one centimeter into the slab, at a time $t = 0.035$ sh, as the size of the zone is refined. The data points fit a quadratic very well, demonstrating that the error scales as the square of the size of the zone.

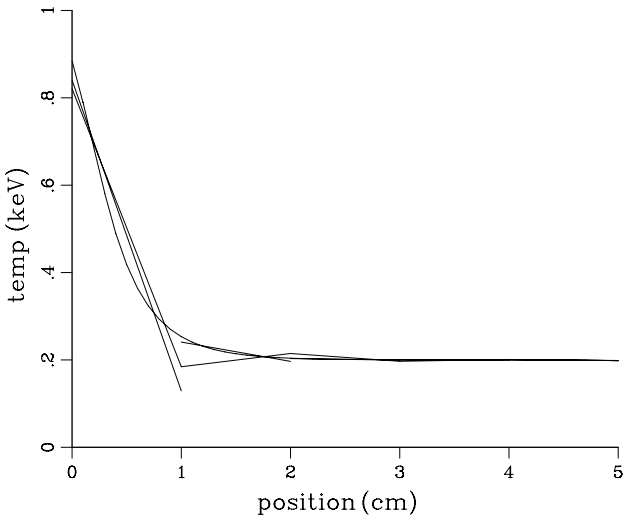

Fig. 6. A calculation showing the effect of enforcing continuity, at a time $t = 0.035$ sh. The discontinuous five zone solution is shown as well as the continuous five zone solution. The smooth curve is the converged 50 zone solution.

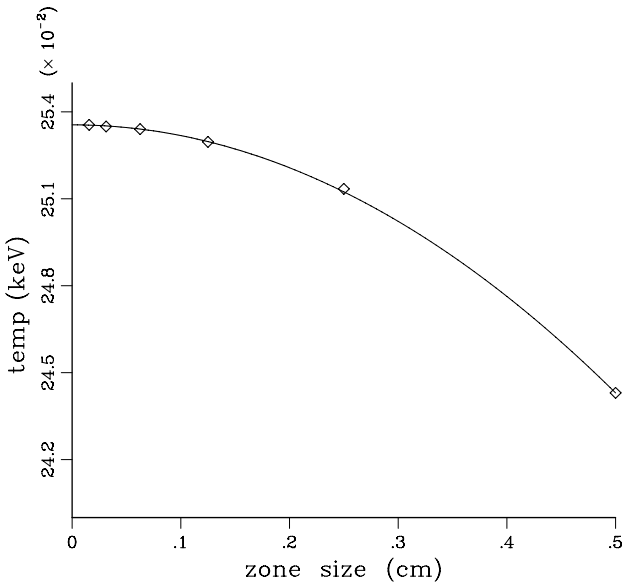

Fig. 7. The temperature of the continuous solution for the problem shown in Fig. 6, at a position of one centimeter and at a time $t = 0.035$ sh, as a function of the zone size. The solid curve is a quadratic fit to the data, $0.25355 - 0.037\mathrm{d}x^2$, demonstrating that the error scales as square of the zone size, dx.

11. Marshak wave propagation in optically thick medium

Up to this point we have explored the characteristics of a number of solution options using problems with an optical thickness of one mean free path per zone. The difference formulation reduces the Monte Carlo noise for optically thick problems, but our prior implementation, which used a piecewise constant treatment of the material temperature, forced calculations to be limited to roughly one mean free path per zone in order to avoid energy teleportation. In this section we explore the behavior of our continuous piecewise linear implementation of the material temperature, T, in the presence of optically thick zones.

Our test problem is, again, Marshak wave propagation into an initially cold medium. For the purpose of this demonstration, we use the continuous basis function set defined in Eq. (55), with conditional lumping of the material energy using the piecewise linear treatment of the temperature. As noted earlier, we lump only the material energy, and in this case we lump the material energy only when a negative temperature excursion would otherwise occur. The mechanism for handling lumping is rather simple. If a negative temperature excursion occurs during an iteration of the Newton–Raphson solution for the temperature, the temperature is set to zero and the lumped form for the material energy in that zone is then used for the remaining iterations. The incident radiation flux is applied to the left side of the problem as a 1 keV blackbody that is turned on at the start of the simulation. The grey opacity of the material is 200 mean free paths per cm, with a specific heat $\rho c_v = 0.1$ (jerk/cc keV) and a time step size of 0.01 sh.

In Fig. 8 we show the material temperature at 30 sh for four instances of the problem, using 10, 20, 40 and 80 zones, respectively. The 10 zone case provides zones that are 100 mean free paths thick, scaling down to the 80 zone case that provides zones that are 12.5 mean free paths thick. The result for the piecewise linear treatment of the temperature, shown in Fig. 8, is in sharp contrast to the behavior of the piecewise constant treatment of the material temperature, shown in Fig. 9. The error in the piecewise constant solution scales roughly linearly with zone size, while the position of the leading edge of the Marshak wave for the piecewise linear treatment, neglecting the foot that must be the size of a zone, appears to be independent of the zone size. This is evidence that our extension of the SIMC method for non-linear time dependent photon transport provides efficient and accurate calculations in thick media.

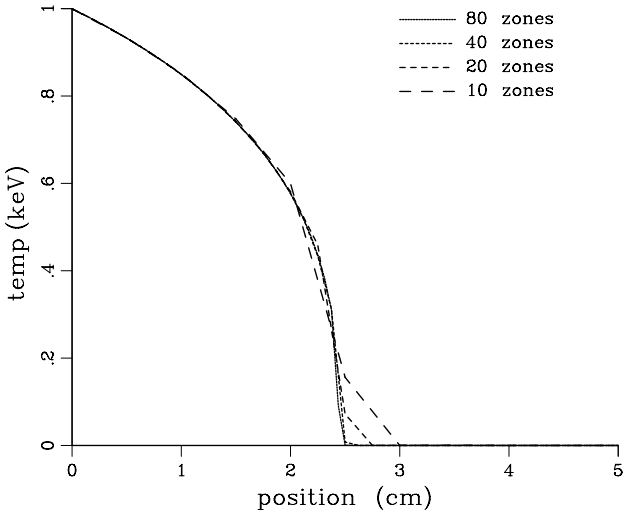

Fig. 8. Marshak wave problem, 200 mean paths per cm. The material temperature at a time $t = 30$ sh is shown. For our piecewise linear solution method, the speed of the wave is independent of the size of the zone.

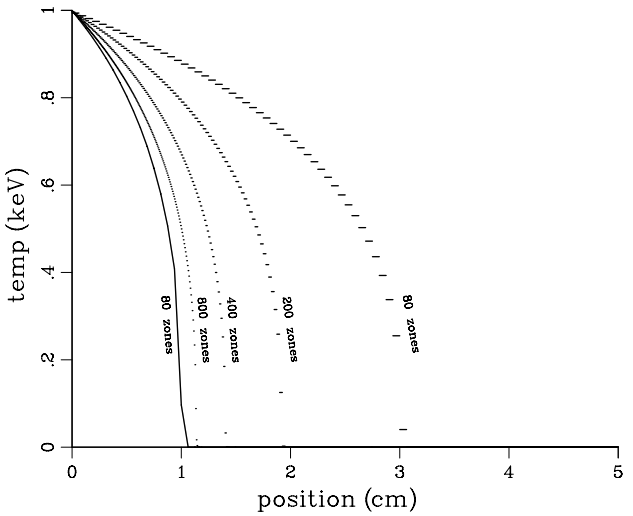

Fig. 9. A Marshak wave problem, 200 mean paths per cm, comparing the piecewise constant implementation of the difference formulation to the piecewise linear implementation. The material temperature at $t = 5.0$ sh is shown. The piecewise constant curves are for 80, 200, 400 and 800 zone solutions, from the right to the left in the plot. The solid line is the 80 zone piecewise linear solution.

12. Discussion

We have extended the piecewise linear treatment of the material state variable for the Symbolic Implicit Monte Carlo (SIMC) transport method, originally developed by Clouet and Samba [7], to the case of the non-linear time dependent equations of photon transport, under conditions of local thermodynamic equilibrium (LTE), in the difference formulation. The use of the difference formulation removes two hurdles that prevent practical application of the method for the standard formulation of photon transport: the difficulty of sampling a transport source term that depends upon the material opacity at the location sampled, and the Monte Carlo noise that becomes an impasse when attempting to use the method in thick media.

In constructing a solution to the non-linear transport problem, one has the choice of linear treatment of the source terms and non-linear treatment of the material energy; or non-linear treatment of the source terms and linear treatment of the material energy. In implementing time dependent solutions for problems involving steep gradients, thermal or Marshak waves, we find that the lack of monotonicity occurring in similarly treated heat flow problems also occurs in radiation transport, and that the technique of lumping the material energy is effective in resolving the difficulty. We lump the material energy in only those zones and time steps where the consistent treatment of the material energy would produce a negative temperature excursion. This only occurs near the leading edge of a Marshak wave as it propagates through cold material. The need to lump the material energy in the presence of steep gradients produces a preference for a linear treatment of the material energy.

In addition to the original discretization method of Clouet and Samba, we have developed a method of enforcing continuity at the interfaces between interior zones; it is appropriate when the material opacity is not discontinuous. It reduces the number of variables that one must solve for and reduces the problem with monotonicity, although it does not remove it. Enforcing continuity between two zones with markedly different material properties would not allow correct treatment of the boundary layer and discontinuity that might appear in the continuum limit. In this case, one allows the discontinuity by not collapsing the matrix at the interface in question.

The SIMC implementation of the solution to the coupled transport and material energy equations does require the construction of a non-linear system that must be solved, involving the influence matrices formed by tracking Monte Carlo particles born during the current time step to remotely located zones where they deposit energy. The dimension of an influence matrix scales with the total number of temperature unknowns in the problem. The bandwidth of the matrix is controlled by the size of the time step, relative to the light travel time between zones, and by the optical thickness of the problem that allows one to stop tracking a particle when its weight has become too small. We do not focus on the issues of solving this non-linear system in this paper, but practical application of the method would obviously be required to do so. We would like to note that collapsing the matrix, to produce the continuous solution where it is appropriate, drops the size of the non-linear system.

In the results we have presented, time was discretized in an implicit piecewise constant manner, producing first order accuracy in the time integration. The basis function approach can be applied to the temporal treatment of the strength of the source terms and it is possible to sample this treatment of the source terms using the SIMC method. Full exposition and evaluation of this extension is beyond the scope this paper, although it follows from the methods we describe in a straightforward manner. We plan to provide an exposition of the extension to piecewise linear time treatment, and computational results, in future work.

Our piecewise linear SIMC treatment of photon transport in the difference formulation produces exceptional performance in the diffusion limit, while offering seamless, accurate, treatment in optically thin portions of a problem. The propagation speed of a Marshak wave in optically thick media is independent of the zone size, while the piecewise constant SIMC treatment requires a per-zone optical thickness of less than one mean free path in order to produce a solution that approximates the correct speed of propagation.

We have explored the properties of our piecewise linear SIMC treatment of the difference formulation for a constant opacity, as a function of temperature and frequency, and for static material without physical scattering. Note that the source terms in the difference formulation are independent of the material opacity; they depend only upon the space and time derivatives of the material temperature. Therefore, inclusion of a realistic material opacity only modifies the exponentiation and energy deposition of Monte Carlo particles as they are propagated, posing no additional difficulties in the source terms. The inclusion of physical scattering, likewise, poses no additional difficulty for the difference formulation.

The piecewise linear treatment of the difference formulation provides an accurate transport technique that is capable of robustly addressing problems in both optically thin, and optically thick, materials. It is capable of producing accurate transport solutions in the diffusion limit. An open question is whether or not the technique referred to as source tilting, that is used in the Implicit Monte Carlo (IMC) [11] method in order to improve the behavior of that algorithm for thick systems, can be used in the SIMC treatment of the difference formulation, and whether it will provide accuracy similar to the self-consistent treatment at a lower computational cost. We plan to explore this possibility in the future.

Acknowledgement

The authors would like to thank Bret Beck for assistance with Monte Carlo sampling issues.

Appendix A. Spatial sampling for linear temperature

As noted earlier, we have multiple terms in the expansion of T in the finite element basis functions. These terms each have unique spatial distribution functions from which we wish to sample. According to [12], the standard method for sampling such a distribution function is:

(1) Integrate the probability density function (p.d.f) to obtain a cumulative distribution function (c.d.f.).
(2) Invert the c.d.f.
(3) Pass to this inverted c.d.f. a uniform random number between 0 and 1 in order to generate a value sampled according to the p.d.f.

Acknowledging that there are other approaches to sampling, for instance rejection techniques, this will be our plan of attack. We list the c.d.f.s of our normalized distribution functions below:

$$\frac{4}{\Delta x}\int_0^y \chi_1^3\,\mathrm{d}x = \frac{4y}{\Delta x} - \frac{6y^2}{\Delta x^2} + \frac{4y^3}{\Delta x^3} - \frac{y^4}{\Delta x^4}, \tag{57}$$

$$\frac{12}{\Delta x}\int_0^y \chi_1^2\chi_2\,\mathrm{d}x = \frac{6y^2}{\Delta x^2} - \frac{8y^3}{\Delta x^3} + \frac{3y^4}{\Delta x^4}, \tag{58}$$

$$\frac{12}{\Delta x}\int_0^y \chi_1\chi_2^2\,\mathrm{d}x = \frac{4y^3}{\Delta x^3} - \frac{3y^4}{\Delta x^4}, \tag{59}$$

$$\frac{4}{\Delta x}\int_0^y \chi_2^3\,\mathrm{d}x = \frac{y^4}{\Delta x^4}, \tag{60}$$

$$\frac{5}{\Delta x}\int_0^y \chi_1^4\,\mathrm{d}x = \frac{5y}{\Delta x} - \frac{10y^2}{\Delta x^2} + \frac{10y^3}{\Delta x^3} - \frac{5y^4}{\Delta x^4} + \frac{y^5}{\Delta x^5}, \tag{61}$$

$$\frac{20}{\Delta x}\int_0^y \chi_1^3\chi_2\,\mathrm{d}x = \frac{10y^2}{\Delta x^2} - \frac{20y^3}{\Delta x^3} + \frac{15y^4}{\Delta x^4} - \frac{4y^5}{\Delta x^5}, \tag{62}$$

$$\frac{30}{\Delta x}\int_0^y \chi_1^2\chi_2^2\,\mathrm{d}x = \frac{10y^3}{\Delta x^3} - \frac{15y^4}{\Delta x^4} + \frac{6y^5}{\Delta x^5}, \tag{63}$$

$$\frac{20}{\Delta x}\int_0^y \chi_1\chi_2^3\,\mathrm{d}x = \frac{5y^4}{\Delta x^4} - \frac{4y^5}{\Delta x^5} \tag{64}$$

and

$$\frac{5}{\Delta x}\int_0^y \chi_2^4\,\mathrm{d}x = \frac{y^5}{\Delta x^5}. \tag{65}$$

We must now invert each of these functions. To do so, we employ Newton–Raphson iteration. This method converges rapidly if given a good starting point. Our goal then is to find an approximation for the inverse of these functions that we can use as the starting point for the Newton–Raphson solver. This will allow us to sample these source terms using a single uniform random number, R, such that $0 \leqslant R \leqslant 1$.

A.1. The method

We make three approximations for each of these functions, depending upon the value of the random number, R. If R is small (near zero) or large (near one) we make appropriate approximations. If R is in neither of these regimes, we exploit the fact that these functions are nearly linear within this range. The transition values between a "low," "medium" and "high" value of R are determined experimentally, by graphically displaying

our first guess solutions and the actual function. As our goal is to reduce the number of iterations required by the Newton–Raphson solver, we only need to find a sufficiently good first guess.

Two of these functions, Eqs. (60) and (65), have algebraic inverses. Furthermore, because the basis functions χ_1 and χ_2 are obtained from each other via reflection about the center of a zone, this symmetry can be exploited in the distribution functions for the particle position. We only need to uniquely sample half of the distribution functions. The others may be sampled by exploiting symmetry. For instance, if we look at the left hand side of Eq. (61), we notice that all values for this function have reflected counterparts in Eq. (65). If we sample Eq. (65) and subtract this value from the width of the zone, we obtain a properly sampled value for Eq. (61). By exploiting this symmetry we need to only focus on inverting three of these c.d.f.s. We choose to invert Eqs. (59) and (64). As there is no symmetric counterpart to Eq. (63), our final choice is made for us. The method is identical for each of these functions. We will outline it in the context of Eq. (59) below.

A.2. Approximation for small R

We begin by simplifying the notation. Each time we pass our function a uniform random number, R, such that $0 \leqslant R \leqslant 1$, we return a position in space. So, we drop the normalization constants and let $x = y/\Delta x$ be the fractional position within the zone. Therefore, Eq. (59) becomes

$$R = 4x^3 - 3x^4. \tag{66}$$

We now define a function, $f(R)$, that satisfies the condition $R \cdot f(R) = 4x^3$. We know from Eq. (66) that

$$R = 4x^3 - 3x^4, \tag{67}$$

$$= R \cdot f(R) - 3x^4, \tag{68}$$

$$= R \cdot f(R) - \frac{3x}{4} R \cdot f(R). \tag{69}$$

When R is small, so is x. To first approximation, then, $R \approx 4x^3$ and we invert this to get a value for x. Therefore, Eq. (69) becomes

$$R = R \cdot f(R) - \frac{3}{4} R \cdot f(R) \cdot \left(\frac{R}{4}\right)^{\frac{1}{3}}. \tag{70}$$

We can now solve for $f(R)$:

$$f(R) = \frac{1}{1 - \frac{3}{4}\left(\frac{R}{4}\right)^{\frac{1}{3}}}. \tag{71}$$

Now, recall our goal is an initial guess for x to pass to the Newton–Raphson solver. Letting this guess be x_0, we know from above that $R \cdot f(R) = 4x_0^3$. We can now invert this relation and insert our value for $f(R)$:

$$x_0 = \left(\frac{R}{4 - 3\left(\frac{R}{4}\right)^{\frac{1}{3}}}\right)^{\frac{1}{3}}. \tag{72}$$

When R is sufficiently small, we pass to the Newton–Raphson solver the initial guess, x_0, as given by Eq. (72) above.

A.3. Approximation for R near one

When our value of R is close to one, we use a similar approximation to obtain a value for x_0. We define new variables, d and y such that $R = 1 - d$ and $x = 1 - y$. Since both R and x are near one, d and y are small. Let us take Eq. (66) and substitute our new values for R and x to get a function of d and y:

$$R = 4x^3 - 3x^4, \tag{73}$$

$$1 - d = 4(1 - y)^3 - 3(1 - y)^4. \tag{74}$$

Expansion and simplification yields

$$d = 6y^2 - 8y^3 + 3y^4. \tag{75}$$

Because both y and d are small we drop the higher order terms and let $d \approx 6y^2$. Inverting yields

$$y = \left(\frac{d}{6}\right)^{\frac{1}{2}}. \tag{76}$$

We now have a starting point for the Newton–Raphson iteration

$$x_0 = 1 - y = 1 - \left(\frac{d}{6}\right)^{\frac{1}{2}} = 1 - \left(\frac{(1-R)}{6}\right)^{\frac{1}{2}}. \tag{77}$$

Eq. (77) yields a first guess for the numerical solver given a value of R close to one.

A.4. Results

Fig. 10 shows our first guess for x_0 plotted against the actual converged solution. Graphically, we determined that our small R approximation is good for values of R less than 0.2. Similarly, our near-one solution is good for values above 0.92. Within the region where neither of the discussed approximations is valid, we have made a linear fit to the curve. The equation of this line is $x_0 = 5/9R + 0.31$. With these values for x_0, the Newton–Raphson solver converges typically within two or three iterations. Fig. 11 shows a histogram of the normalized sampling of $\overline{\chi_1\chi_2^2}$ using 100,000 uniform random numbers between zero and one. The actual normalized function ($\overline{\chi_1\chi_2^2} = 12(-x^3 + x^2)$) is also plotted. It is clear that our sampling is accurate, to within sampling noise. As the number of random numbers increases, the histogram converges to the function. Our sampling of the other two functions, Eqs. (63) and (64) is similar.

Appendix B. Improved frequency sampling

In the difference formulation, the source terms are derivatives of the Planck function. In the piecewise constant (in space) discretization there exist discontinuities in Φ both between zones and between time steps. In the piecewise linear (in space) discretization, Φ can still be discontinuous between zones, and in time, leading

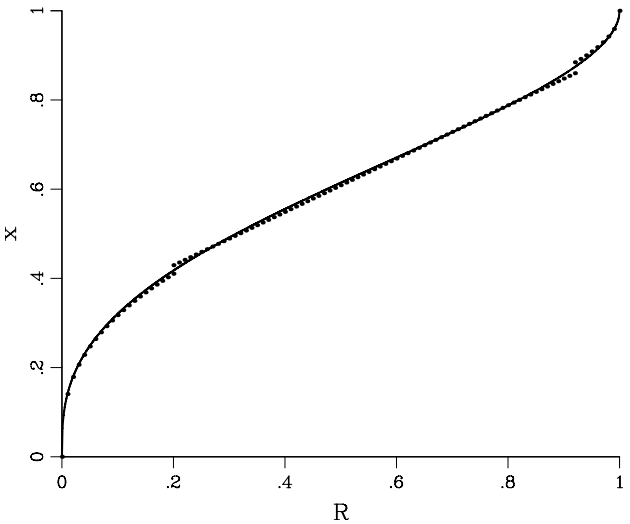

Fig. 10. The first guess for the solution, x_0, using our approximation techniques, shown with the black dots, plotted over the converged c.d.f. shown with the solid black line. Our x_0 is derived differently depending upon the value of R chosen. For small and relatively large values of R, we use the solutions outlined in Appendices A.2 and A.3 respectively. Otherwise we approximate the converged c.d.f. linearly.

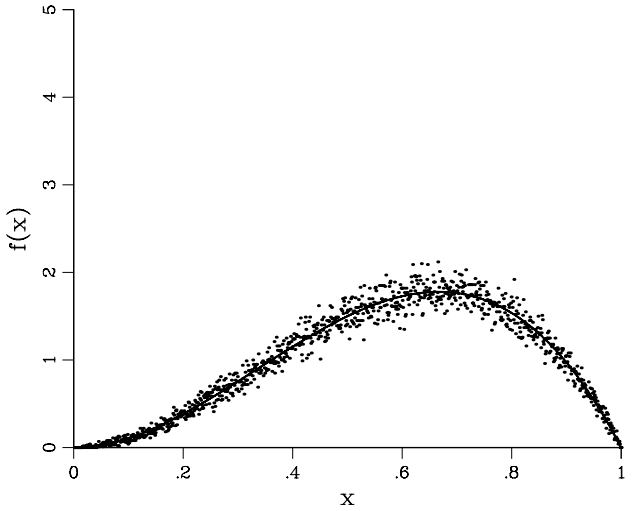

Fig. 11. Our normalized sampling of the function $\overline{\chi_1\chi_2^2}$ with 100,000 random numbers plotted against the actual function. The zone width is taken to be one. The difference between the histogram and the actual function is from sampling error.

to the requirement for sampling $(4\pi/c)(\partial B/\partial\Phi)$ for finite differences. In the appendix of [2] a rejection technique was used to sample the frequency distribution of these sources. Here, we develop an improved method, focusing on the $\partial B/\partial x$ source. The $\partial B/\partial t$ source is similar.

Let us assume that at some position $x = x_i$ the material state variable jumps from Φ_1 to Φ_2. Integrating the $\partial B/\partial x$ source in Eq. (6) shows that

$$-\mu\int_{x_i-\epsilon}^{x_i+\epsilon}\frac{\partial B}{\partial x}\mathrm{d}x = -\mu[B(v,(x_i+\epsilon)) - B(v,(x_i-\epsilon))], \tag{78}$$

where ϵ is a small distance. Now, if we note that the material state variables to the left and right side of the discontinuity are Φ_1 and Φ_2 we can rewrite Eq. (78) as

$$-\mu\int_{\Phi_1}^{\Phi_2}\frac{\partial B}{\partial\Phi}\mathrm{d}\Phi = -\mu[B(v,\Phi_2) - B(v,\Phi_1)]. \tag{79}$$

Now we use the factorization of $B(v,\Phi) = (c/4\pi)b(v,\Phi)\Phi$, Eq. (5), to rewrite Eq. (79), obtaining

$$-\mu\int_{\Phi_1}^{\Phi_2}\frac{\partial B}{\partial\Phi}\mathrm{d}\Phi = -\mu\frac{c}{4\pi}[b(v,\Phi_2)\Phi_2 - b(v,\Phi_1)\Phi_1] = -\mu\frac{c}{4\pi}\left[\frac{b(v,\Phi_2)\Phi_2 - b(v,\Phi_1)\Phi_1}{\Phi_2-\Phi_1}\right](\Phi_2-\Phi_1). \tag{80}$$

Let us call the term in the brackets $f[v,\Phi_1,\Phi_2]$. We now show that $f[v,\Phi_1,\Phi_2]$ is a probability density function. For this, $f[v,\Phi_1,\Phi_2]$ must be strictly positive and integrate to unity for all frequencies.

The first condition is simple: $B(v,\Phi)$ is strictly monotonic in Φ. Namely, if $\Phi_2 > \Phi_1$, then $B(v,\Phi_2) > B(v,\Phi_1)$ for all values of v. As such, the signs of the numerator and denominator of $f[v,\Phi_1,\Phi_2]$ will always match. Therefore, $f[v,\Phi_1,\Phi_2]$ will be positive for all values of v.

To demonstrate the second condition, we integrate $f[v,\Phi_1,\Phi_2]$ over all frequencies

$$\begin{aligned}\int_0^\infty f[v,\Phi_1,\Phi_2]\,\mathrm{d}v &= \int_0^\infty\left[\frac{b(v,\Phi_2)\Phi_2 - b(v,\Phi_1)\Phi_1}{\Phi_2-\Phi_1}\right]\mathrm{d}v\\ &= \frac{1}{\Phi_2-\Phi_1}\left[\int_0^\infty b(v,\Phi_2)\Phi_2\,\mathrm{d}v - \int_0^\infty b(v,\Phi_1)\Phi_1\,\mathrm{d}v\right].\end{aligned} \tag{81}$$

Using Eq. (4), we get our result

$$\int_0^\infty f[v,\Phi_1,\Phi_2]\,\mathrm{d}v = \frac{1}{\Phi_2-\Phi_1}[\Phi_2-\Phi_1] = 1. \tag{82}$$

Therefore, $f[v, \Phi_1, \Phi_2]$ is a probability density function for frequencies.

We need a way to sample $f[v, \Phi_1, \Phi_2]$. If we rearrange Eq. (80) we get

$$f[v, \Phi_1, \Phi_2] = \frac{1}{\Phi_2 - \Phi_1} \int_{\Phi_1}^{\Phi_2} \left[\frac{4\pi}{c} \frac{\partial B}{\partial \Phi}\right] \mathrm{d}\Phi. \tag{83}$$

This means that the frequency distribution for a finite jump across a boundary is an average of the term in the brackets in Eq. (83) over the jump in Φ. It can be found by Monte Carlo averaging over the interval in Φ. Our algorithm to do so employs a few steps:

(1) Sample a value of Φ uniformly on the interval $[\Phi_1, \Phi_2]$.
(2) From this Φ_{sample}, calculate the corresponding $T_{\text{sample}} = (\Phi_{\text{sample}}/a)^{1/4}$.
(3) Sample the term in the brackets of Eq. (83), returning a value for v_{sample} according to this distribution. This is done using the method described in the appendix of [2].

Fig. 12 shows the results of our sampling of $f[v, \Phi_1, \Phi_2]$ plotted against the function $f[v, \Phi_1, \Phi_2]$ for different values of Φ_1 and Φ_2. There is excellent agreement between the sampling and the distribution function in all

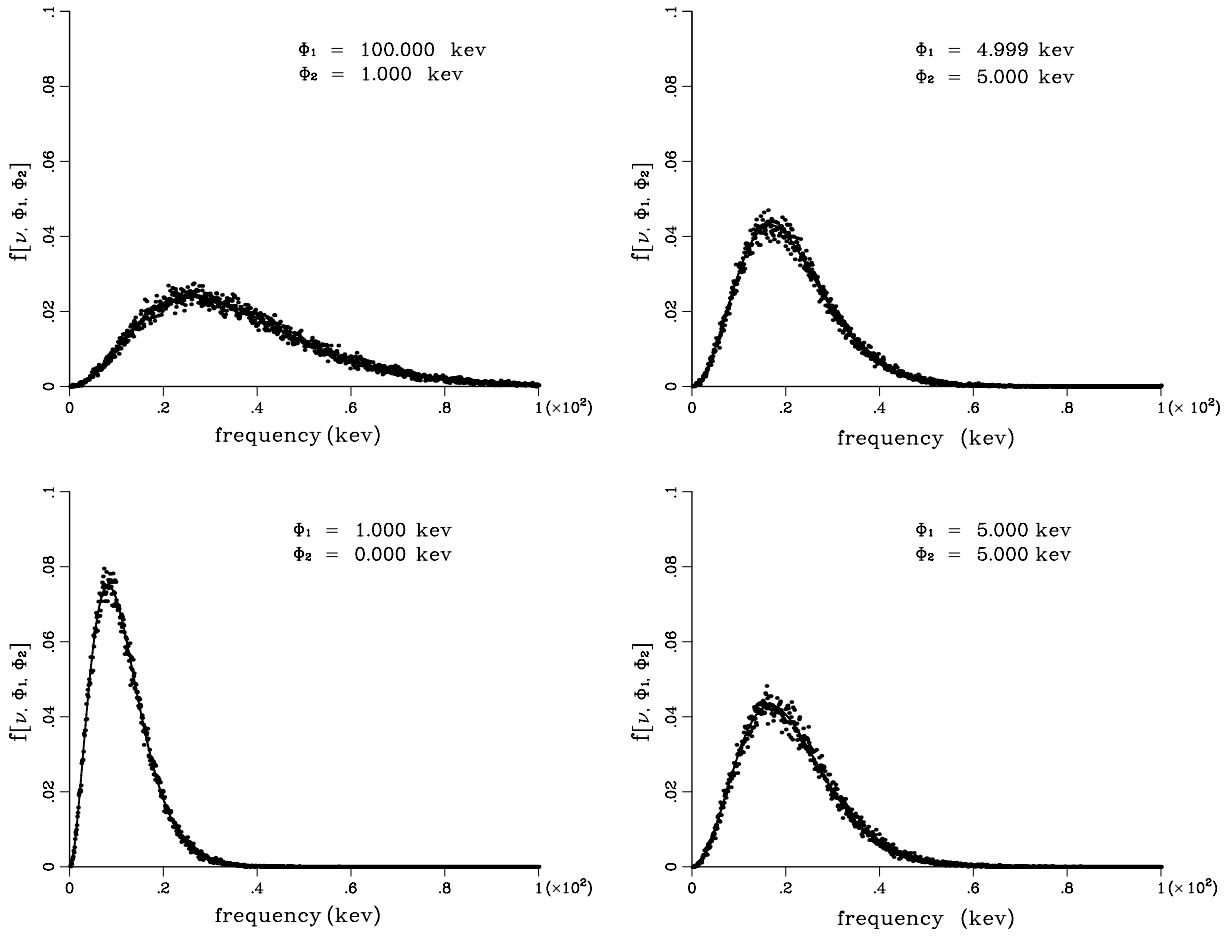

Fig. 12. Our normalized sampling of the function $f[v, \Phi_1, \Phi_2]$ with 100,000 random numbers plotted against the actual function for varying values of Φ_1 and Φ_2. Our sampling is accurate when the two temperatures are close together or far apart, as shown in the upper right and upper left plots, respectively, regardless of whether Φ_1 or Φ_2 has the larger value. The bottom left plot shows accuracy when one temperature is zero. In this case, we are plotting $b(v, \Phi_1)$. When the two temperatures are identical, the drawn function is $(4\pi/ca)\partial B/\partial\Phi$. Even in this case, our histogram matches well.

cases. Our histograms have been scaled to have unit area, whereas $f[v, \Phi_1, \Phi_2]$ is already normalized. In the case where $\Phi_1 = \Phi_2$, $f[v, \Phi_2, \Phi_1]$ is undefined. However, as described in the appendix of [2],

$$\lim_{\Phi_1 \to \Phi_2} \frac{b(v, \Phi_1)\Phi_1 - b(v, \Phi_2)\Phi_2}{(\Phi_1 - \Phi_2)} = \frac{4\pi}{ca} \frac{\partial B(v, T)}{\partial T^4}. \tag{84}$$

Thus, we plot the function $[4\pi/ca][\partial B(v, T)/\partial T^4]$ against our histogram in the bottom right of Fig. 12. Our sampling algorithm does not change at all. This new method of sampling is both robust and accurate, handling all limiting cases. Our two temperatures, Φ_1 and Φ_2, can be close together, far apart, identical or zero. We do not need to employ a rejection technique, nor check the ratio of the two temperatures, to accurately sample the frequency distribution.

References

[1] A. Szőke, E.D. Brooks III, The transport equation in optically thick media, Journal of Quantitative Spectroscopy and Radiative Transfer 91 (2005) 95–110.
[2] E.D. Brooks III, M.S. McKinley, F. Daffin, A. Szoke, Symbolic Implicit Monte Carlo radiation transport in the difference formulation: a piecewise constant discretization, Journal of Computational Physics 205 (2005) 737–754.
[3] E.D. Brooks III, Symbolic Implicit Monte Carlo, Journal of Computational Physics 83 (1989) 433–446.
[4] T. N'kaoua, Solution of the nonlinear radiative transfer equations by a fully implicit matrix Monte Carlo method coupled with the Rosseland diffusion equation via domain decomposition, SIAM Journal on Scientific and Statistical Computing 12 (1991) 505.
[5] M.S. McKinley, E.D. Brooks, A. Szoke, Comparison of implicit and Symbolic Implicit Monte Carlo line transport with frequency weight vector extension, Journal of Computational Physics 189 (2003) 330–349.
[6] J.D. Densmore, E.W. Larsen, Asymptotic equilibrium diffusion analysis of time-dependent Monte Carlo methods for grey radiative transfer, Journal of Computational Physics 199 (2004) 175–204.
[7] J.-F. Clouet, G. Samba, Asymptotic diffusion limit of the symbolic Monte-Carlo method for the transport equation, Journal of Computational Physics 195 (2004) 293–319.
[8] B. Su, G.L. Olson, Benchmark results for the non-equilibrium Marshak diffusion problem, Journal of Quantitative Spectroscopy and Radiative Transfer 56 (1996) 337–351.
[9] E.W. Larsen, The asymptotic diffusion limit of discretized transport problems, Nuclear Science and Engineering 112 (1992) 336–346.
[10] G. Strang, G.J. Fix, An Analysis of the Finite Element Method, Prentice-Hall, 1973.
[11] J.A. Fleck Jr., E.H. Canfield, A random walk procedure for improving the computational efficiency of the implicit Monte Carlo method for nonlinear radiation transport, Journal of Computational Physics 54 (1984) 508–523.
[12] M.H. Kalos, P.A. Whitlock, Monte Carlo Methods, John Wiley and Sons, New York, 1986.